PARAMETRIC ANALYSIS OF FISCHER-TROPSCH SYNTHESIS IN A CATALYTIC MICROCHANNEL REACTOR

by

Gamze Gümüşlü

B.S., Chemical Engineering, Boğaziçi University, 2008

Submitted to the Institute for Graduate Studies in
Science and Engineering in partial fulfillment of
the requirements for the degree of
Master of Science

Graduate Program in Chemical Engineering

Boğaziçi University

2010

PARAMETRIC ANALYSIS OF FISCHER-TROPSCH SYNTHESIS IN A CATALYTIC MICROCHANNEL REACTOR

APPROVED BY:

Assoc. Prof. Ahmet Kerim Avcı (Thesis Supervisor)	.....
Assoc. Prof. Hasan Bedir	.....
Prof. Zeynep İlsen Önsan	.....

DATE OF APPROVAL: 15.06.2010

ACKNOWLEDGEMENTS

I would like to express my sincere thanks to my supervisor Assoc. Prof. Ahmet Kerim Avcı, not only for guiding me all through this research but also for encouraging me to start and pursue my M.Sc. degree. It was a pleasure to work with him both in my undergraduate and graduate educations.

I also would like to thank to my thesis committee members, Prof. Zeynep İlsen Önsan and Assoc. Prof. Hasan Bedir for devoting their valuable time to read and comment on my thesis.

I wish to thank to Seda Aktaş for the congenial friendship and the help she provided as a mate in KB "404". I offer many thanks to Melek Selcen Başar for her friendship, help and support especially during the time we spent in graduate education. Likewise, I should thank to Aysun İpek Paksoy. I have heartfelt appreciation for both Selcen and İpek as they rendered each day in KB more enjoyable. I am also grateful to Mustafa Karakaya for sharing his software knowledge for my thesis.

Though I do not know how to, I want to express my deepest gratitude to my family for always being there for me, supporting me and encouraging me for the next step throughout my life. I feel a great indebtedness to my family since I wouldn't have come this far without them. This thesis is dedicated to them.

Finally, I would like to acknowledge TUBITAK for granting me a M.Sc. degree scholarship. Financial support is provided by Boğaziçi University Research Fund through project BAP-09HA507D and by TUBA-GEBIP program.

ABSTRACT

PARAMETRIC ANALYSIS OF FISCHER-TROPSCH SYNTHESIS IN A CATALYTIC MICROCHANNEL REACTOR

Fischer-Tropsch synthesis (FTS) is the catalytic conversion of synthesis gas, which is a mixture of carbon monoxide and hydrogen, to a wide range of synthetic fuels that can replace their petroleum-driven counterparts. FTS requires effective temperature control since the product distribution strongly depends on temperature. Integration of FTS with microchannel reactor technology can turn into a promising process, since sub-millimeter dimensions of this technology lead to significant intensification of the process that inherently minimizes transport resistances and allows excellent temperature control and efficient use of the catalyst. The aim of this study is to analyze FTS in catalytic microchannels through a parametric analysis employing computer-based techniques and to explore the effects of reactor geometry and operating parameters on FTS temperature. For this purpose, FTS is to run at high temperature (623 K) and pressure (20 atm) over a Fe-Cu-K catalyst in a microchannel network composed of horizontal arrays of reaction and cooling channels. The two dimensional geometry is simulated by COMSOL Multiphysics^{TM} using finite element method. Analysis is based on exploring the effects of material type and thickness of the separating wall, side length of the cooling channel, the type and flow rate of cooling fluid, molar H_2/CO ratio in the feed and channel wall texture on the FTS temperature.The results indicate that, using thicker walls with high thermal conductance properties and micro-baffles on the catalytic wall can lead to near-isothermal conditions during FT operation. In contrast with the type and flow rate of the coolant, cooling channel side length is found to have negligible effect on the reaction temperature. It is observed that increasing H_2/CO ratio leads to a decrease in average temperature.

ÖZET

FISCHER-TROPSCH SENTEZİNİN KATALİTİK MİKROKANAL REAKTÖR ÜZERİNDE PARAMETRİK ANALİZİ

Fischer-Tropsch sentezi (FTS), karbon monoksit ve hidrojen gazlarının karışımından oluşan sentez gazının katalizör eşliğinde petrol bazlı pek çok yakıtın muadili olabilecek sentetik yakıtlara dönüştürülmesidir. FTS sonucu oluşan ürünlerin dağılımı ortam sıcaklığına bağlı olduğundan, etkin sıcaklık kontrolü gerekmektedir. Bu noktada, FTS ile mikrokanal reaktör teknolojisinin birleştirilmesi başarılı sonuçlar verebilir; mikrometre civarındaki boyutlarıyla mikrokanal teknolojisi, hem süreçlerde küçülmeyi hem de kütle ve ısı iletimi dirençlerinin en düşük seviyeye indirebilmesini, aynı zamanda katalizörün etkin biçimde kullanımını sağlayabilmektedir. Bu çalışmada, FTS nin katalitik mikrokanallardaki davranışı, bilgisayar destekli yöntemlerle parametrik olarak incelenmiş, reaktör geometrisi ve çalışma şartlarının FT sıcaklığı üzerindeki etkileri araştırılmıştır. Yüksek sıcaklık (623 K) ve basınçta (20 atm) ilerleyen FTS, yatay dizilerden oluşmuş mikrokanal ağı içerisinde soğutucu kanallarla eşleştirilmiştir. İki boyutlu olarak oluşturulan geometri COMSOL Multiphysics^{TM} kullanılarak sonlu elemanlar yöntemiyle çözülmüştür. Parametrik analiz, kanalları ayıran duvarın malzeme türü ve kalınlığının, soğutma kanalını çapının, soğutucu türü ve akış hızının, girişteki molar H_2/CO oranının ve kanal duvarı şeklinin FT kanal sıcaklığı üzerindeki etkilerinin incelenmesine dayanmaktadır. Sonuçlar, kalın, yüksek iletkenlikli ve reaksiyon tarafında mikro-girintili duvar kullanımıyla FT kanalında sabite yakın sıcaklıklar elde edilebileceğini göstermektedir. Ayrıca, soğutma kanal çapı değişimi sıcaklık üzerinde kayda değer bir etki göstermezken, soğutucu çeşidi ve miktarının önemli değişikliklere yol açtığı görülmektedir. H_2/CO oranının arttırılmasıyla FT kanalında düşük sıcaklıklara ulaşılabileceği gözlenmiştir.

TABLE OF CONTENTS

LIST OF FIGURES

LIST OF TABLES

LIST OF SYMBOLS/ABBREVIATIONS

A_c	Cross-sectional area of wall
c_A	Concentration of species A
$\overline{c}_A$	Average concentration of species A
C_P	Heat capacity of species
D	Hydraulic diameter of channel
D_{AB}	Diffusion coefficient of A in B
$D_{AB,eff}$	Effective diffusion coefficient in catalyst layer
dL	Length increment
dS	Area increment
E_5	Activation energy for paraffin formation (n≥2)
E_{5M}	Activation energy for methane formation
E_6	Activation energy for olefin formation (n≥2)
E_v	Activation energy for WGS reaction
F_A	Flow rate of species A
$\overline{F}_A$	Average flow rate of species A
F_{A0}	Initial flow rate of species A
F_{HC}	Total hydrocarbon molar flow
h	Heat transfer coefficient
i	Species index
j	Species index
k_{eff}	Effective thermal conductivity in catalytic
k_i	Thermal conductivity of the gas in channel i
k_{mix}	Thermal conductivity of mixture
k_{wall}	Thermal conductivity of the wall
k_1	Rate constant of CO adsorption
k_5	Rate constant of paraffin formation
$k_{5,0}$	Preexponential factor of paraffin formation (n≥2)
k_{5M}	Rate constant of methane formation
$k_{5M,0}$	Preexponential factor of rate constant of methane formation

k_6	Rate constant of olefin desorption reaction
$k_{6,0}$	Preexponential factor of rate constant of olefin desorption reaction
k_v	Rate constant of CO_2 formation
$k_{v,0}$	Preexponential factor of rate constant of CO_2 formation
k_{-6}	Rate constant of olefin re-adsorption reaction
K_2,K_3,K_4	Equilibrium constants of elementary reaction steps for FTS reactions
K_P	Equilibrium constant of WGS reaction
K_v	Group of constants in WGS reaction
L	Channel length
m	Channel index
M	Molecular mass
$\dot{m}$	Mass flow rate
Mw	Molecular weight
N	Maximum carbon number of the hydrocarbons involved
n	Carbon number
Nu	Nusselt number
P	Total pressure
P_A	Partial pressure of species A
P_i	Partial pressure in channel i
Pr	Prandtl number
q	Total number of species
Q	Generated heat
R	Universal gas constant
r_A	Rate of formation of species A
R_{CH_4}	Rate of formation of CH_4
$R_{C_{2n}H_{2n}}$	Rate of formation of olefins
$R_{C_{2n}H_{2n+2}}$	Rate of formation of paraffins
R_{CO_2}	Rate of formation of CO_2
Re	Reynold's number
S	Sutherland's constant

S	Cross sectional are of the channel
T	Temperature
$\overline{T}$	Average temperature
T_{ave}	Average temperature
T_i	Temperature within channel i
T_w	Temperature of within the wall
T_0	Initial, reference temperature
u	Linear velocity
v_i	Linear velocity in channel i
$\overline{v}$	Average linear velocity
$v_{i,0}$	Initial linear velocity in channel i
v_x	x component of linear velocity
$v_{x,i}$	x component of linear velocity in channel i
v_y	y component of linear velocity
$v_{y,i}$	y component of linear velocity in channel i
V_0	Volumetric flow rate
w	Weight fraction
x	Mole fraction
X_{CO}	Carbonmonoxide conversion
y_{A0}	Initial mole fraction of species A
α	Thermal diffusivity
α	chain growth probability
α_n	Chain growth factor for carbon number of n (n≥2)
α_A	Chain growth probability in the Anderson-Schulz-Flory distribution
α_1	Chain growth factor for carbon number of 1
β_n	Re-adsorption factor of 1-olefin with carbon number of n
δ	Constant in the heat capacity equation
ΔH_A	Heat of formation of A at T
ΔH_{A0}	Standard heat of formation of A
γ	Constant in the heat capacity equation

ε_p	Porosity of washcoat layer
κ	Permeability of washcoat layer
λ	Conduction parameter
μ	Viscosity
μ_b	Bulk viscosity
μ_{mix}	Viscosity of mixture
μ_0	Viscosity at average wall temperature
μ_0	Viscosity at reference temperature T_0
ρ	Density
τ	Tortuosity of washcoat layer
σ	Stoichiometric coefficient
φ	Constant in the heat capacity equation
ϑ	Structural volume increment
ξ	Constant in the heat capacity equation

CFD	Computational fluid dynamics
cool	Cooling channel
FTS	Fischer-Tropsch Synthesis
HC	Hydrocarbon
HTFT	High temperature Fischer-Tropsch
LTFT	Low temperature Fischer-Tropsch
O/P	Olefin to paraffin ratio
rxn	Reaction channel
STP	Standard temperature and pressure
WGS	Water-gas shift

1. INTRODUCTION

Petroleum crude oil is an important commodity since it has been used in energy generation as a fuel and in the production of many chemicals as a raw material. However, as the price of crude oil is increasing and the natural resources of crude oil are becoming depleted, production of synthetic hydrocarbons by Fischer-Tropsch (FT) synthesis is becoming more important (Dry, 1999; Dry, 2002). Fischer-Tropsch synthesis is a collection of a series of reactions which converts synthesis gas, a mixture of CO and H_2, to a range of hydrocarbons in the presence of iron, cobalt or ruthenium catalysts (Schulz, 1999; Van der Laan and Beenackers, 1999b). As synthesis gas generation does not depend on petroleum, and can be produced from natural gas, coal or biomass, FT synthesis offers an alternative, petroleum-free route to producing commodity fuels such as gasoline and diesel (Aasberg-Petersen *et al.*, 2004; Mazonne and Fernandes, 2006).

The most important factor in Fischer-Tropsch synthesis is the product selectivity, which is greatly influenced by the process conditions, namely by temperature, partial pressures of H_2 and CO in feed and space velocity (Steynberg, 2004). It is confirmed by many studies in literature that the impact of process temperature is much more significant than any other operating condition (Schulz, 1999; Van der Laan and Beenackers, 1999b; Dry, 2002). Therefore, in order to obtain hydrocarbons in the desired type and carbon-number range, it is essential to have robust temperature control of the synthesis reaction. At this point, process intensification by using micro-structured equipments may be a way of achieving desired temperature control in Fischer-Tropsch and optimizing the product selectivity. Process intensification is known as the method of miniaturizing process equipments and plants (Zanfir and Gavriilidis, 2001). Use of micro-structured equipments, such as microchannel reactors and heat exchangers, which are composed of channels of sizes in range of 100 μm to 1mm, enables this intensification (Harris *et al.*, 2000). The advantages of microchannel equipments such as high surface to volume ratios up to 50,000 m^2/m^3, improved heat and mass transfer characteristics, safer operation and shorter residence time distribution make them to

be considered as processing units to achieve better results in Fischer-Tropsch synthesis in terms of the product selectivity (Kiwi-Minsker and Renken, 2005; Van Male *et al.*, 2004).

The aim of the present work is to investigate the response of Fischer-Tropsch synthesis in a catalytic microchannel reactor against changes in the geometric configurations and in operating conditions through a series of parametric analyses. In these studies, only paraffin and olefin producing reactions and water gas shift (WGS) reaction are assumed to occur within the reaction channel. The reaction system is considered to be a microchannel network composed of adjacent channels in form of parallel arrays, which are arranged such that the coolant and reaction mixtures flow in successive flow paths. With this configuration it is aimed to control the temperature of the reaction channel and also to simplify the modeling of the system; based on the fact that same reaction is occurring or cooling fluid is flowing within the parallel groups of channels, the heat flow between identical channels is assumed to be negligible compared to heat flow between successive 'reaction-cooling' channels, allowing elimination of one spatial dimension from the calculations. The resulting two-dimensional momentum, mass and energy transport equations forming a set of partial differential equations are solved in COMSOL Multiphysics package using finite element method. The catalyst, industrial Fe-Cu-K (Wang *et al.*, 2003), is considered as a washcoated, porous layer on the walls of reaction channels where Brinkman type equations are used to model the reactive flow.

Parametric study is conducted through making changes in the material and thickness of the wall separating coolant and reaction channels, side length of the cooling channel, the type and flow rate of coolant fluid, molar H_2/CO ratio in the feed and channel wall texture and observing the effects on the FT channel temperature and the product distribution. Hydrocarbon products are taken as the alkanes and alkenes in the range of C_1 and C_7. This range is mainly composed of fuel gas, LPG and gasoline (Van der Laan, 1999). CO_2 and H_2O are other products formed by the synthesis reactions. H_2, which constitutes a great amount of feed syngas, is also produced as a result of the water-gas shift reaction.

The literature survey on Fischer-Tropsch synthesis and microchannel technology is given in Chapter 2. Mathematical modeling and simulation of the microchannel system are presented in Chapter 3.Chapter 4 includes the results of simulations and the discussion of the results. Major outcomes of the study and recommendations for possible future work are presented in Chapter 5.

2. LITERATURE SURVEY

2.1. Microstructured Systems

In order to meet the increasing demands and to reduce their operating expenses, plants are seeking novel methods of production technologies. When considered in the context of conventional techniques, the novelties will be limited in terms of cost, size, utility, control. However, with the concept of process intensification, it is aimed to miniaturize the equipments, which can lead to significant size reductions and, consequently, to reduced capital and operating expenses together with safe, efficient and lower-emission operations (Zanfir and Gavriilidis, 2000). Miniaturized systems also mean that the plant can be transportable by any means if necessary (Seris *et al.*, 2008).

The concept of miniaturizing can be achieved by using Microstructured Reactors (MSRs). These units consist of open paths or channels for fluid flow with dimensions at the sub-millimeter range. Most of the MSRs are composed of multiple parallel channels with diameters 10 to several hundred micrometers and usually, the flow through these channels are in laminar flow conditions (Renken and Kiwi-Minsker, 2005). Microchannel units are also used as heat exchangers with dimensions varying between 100 μm - 1mm (Harris *et al.*, 2000).

Most of examples for microstructured units are laboratory scale productions especially for hazardous chemical operations like phosgene synthesis or for hydrogen production which is used in driving proton exchange membrane fuel cells. Microchannel systems are becoming popular and only a few attempts are made to convert the lab-scale results into industrial-scale production. One of the demonstrated projects about potential usage of MSR is epoxidation of propylene with hydrogen peroxide (Renken and Kiwi-Minsker, 2005). Another example can be given for water gas shift reaction which is involved in the gas purification operation for steam reforming (Kolb and Hessel, 2004).

2.1.1. Comparison of microstructured and conventional systems

Microstructured reactors and heat exchangers are getting more recognized in the literature as well as in the chemical process industries. In a world where capital required to sustain world-scale production of chemicals cannot be provided by many developing countries, plants with units composed of microchannels became very important (Seris *et al.*, 2008). Advantages of using microstructured devices instead of conventional sized equipments can be explained with higher surface to volume ratio, better heat and mass transfer, safer operation, easier scaling up, better temperature control, lower installation cost (Tonkovich *et al.*, 2004).

One of the most important benefits of micro-sized units is their high surface area to volume ratio; this value is in range of 10,000-50,000 m^2/m^3 for a unit (reactor or heat exchanger) composed of parallel microchannels, whereas the ratio is mostly around 100 m^2/m^3 and rarely exceeds 1,000 m^2/m^3 in conventional units (Ehrfeld *et al.*, 1999). This significant difference in compactness allows very fast heat transfer rates which is critical in highly exothermic and endothermic reactions in terms of both catalyst utilization and of preventing formation of hot-spots. Since heat transfer coefficient is very high in these reactors, it is possible to achieve enhanced heat transfer with these units (Kiwi-Minsker and Renken, 2005).

Mass transfer, just like heat transfer, is better in microreactors. The flow amount and sizes of channels are small and, hence, the flow turns out to be in laminar regime. This means that flow is more in order showing fewer fluctuations and causing less pressure drop (Tonkovich *et al.*, 2004; Tonkovich *et al.*, 2007). Since laminar flow is fully developed in microchannels the Sherwood number, which is mass transfer coefficient multiplied by hydraulic diameter divided by the diffusion coefficient, reaches a constant value. This implies that as the hydraulic diameter gets smaller; the mass transfer coefficient gets larger, decreasing the mass transfer limitation (Fichtner *et al.*, 2001). Except from checking Sherwood number, other criteria were applied in some other studies; Görke *et al.* (2002) applied Mears criterion, Commenge *et al.* (2002) used Damköhler number, Ajmera *et al.* (2002) applied Weisz-modulus. In all of these

studies, it was reported that mass transfer was not limiting the performance of the reactor (Kolb and Hessel, 2004).

In addition to significant compactness and related improvements in heat and mass transfer rates, small channel diameters facilitate shorter diffusion times which results in obtaining shorter residence time distribution (RTD). The importance of RTD arises from the fact that in processes composed of successive reactions, it is possible to achieve high selectivity of the desired products, such as intermediates, with shorter RTDs (Kiwi-Minsker and Renken, 2005). This property is crucial for industries such as production of pharmaceuticals and fine chemicals, which heavily demand selective production of target products.

Compared to conventional units, hold-up (amount of reactant/product flow) in the microchannels is considerably small (Kiwi-Minsker and Renken, 2005). This feature gives the opportunity of safe operations in the reactions characterized by near-explosive conditions, such as direct partial oxidation of hyhdrocarbons to synthesis gas (Veser and Frauhammer, 2000; Veser, 2001). Apart from the operational benefits, scaling-up the microchannel reactors is much easier than the conventional units. A multichannel unit is characterized by a single channel; the reaction physics and flow properties in one channel will be the same in the others, provided that feed is uniformly distributed to every channel (Tonkovich *et al.*, 2005). As a result, the reactor can be sized-up simply by calculating the total number of channels to give the desired throughput (Hasebe, 2004). In other words, scale-up is done via increasing the number of microchannels without changing the geometry of the unit cell, which is called "numbering-up" (Kolb and Hessel, 2004).

Although there are many advantages of microstructured units, there exist some challenging features. First of all, it is difficult to introduce solid catalysts into microchannels and channels are very sensitive to precipitating products since presence of solid particles brings up the possibility of plugging of the channel (Geyer *et al.*, 2006; Holladay *et al.*, 2004; Kiwi-Minsker and Renken, 2005). Using catalyst in packed form increases the possibility of plugging and also cause high pressure drops within the

channel, therefore catalytic wall microreactors are referred as a more suitable option (Holladay *et al.*, 2004; Jensen, 2001; Kiwi-Minsker and Renken, 2005). Other challenges related to microstructured systems to address includes the increased sensitivity of channels to fouling, the difficulty in sealing, the potential of channelling when high amount of throughput is introduced and the difficulties in system monitoring (Holladay *et al.*, 2004). However, microstructure technology is deployed by optimizing the process conditions, reactor geometries such that the advantages provided by microchannels override the challenges (Jensen, 2001; Tonkovich *et al.*, 1999)

The excellent heat and mass transfer characteristics, microchannel technology seems as a viable option to be used with reactions having exothermic and transport limited nature such as Fischer-Tropsch synthesis, which especially requires effective temperature control to determine the product distribution.

2.2. Fischer-Tropsch Synthesis

Fischer-Tropsch synthesis is a combination of reaction series in which synthesis gas, a mixture of carbon monoxide and hydrogen, is converted into aliphatic hydrocarbons, and named after the people, Franz Fischer and Hans Tropsch, who discovered it (Van der Laan and Beenackers, 1999b).

The FT technology development and applications in 1930's in Germany, which took roots from coal utilisation, did not solely depend on economical considerations. They were rather resulted from strategic and political considerations (Steynberg, 2004). However, nowadays, economical considerations are far more important to choose FT synthesis as an alternative route to produce liquid fuels and chemicals (Dry, 1999). It is claimed that using FT synthesis to produce fuels is feasible when the crude oil price exceeds ca.20 dollars per barrel (Dry, 2002; Steynberg, 2004). From Figures 2.1 and 2.2, it can be seen that for almost ten years, price of oil per barrel did not fall below $20. Recently, the price of crude oil per barrel is approximately $80, thus FT synthesis is a viable option for producing fuels.

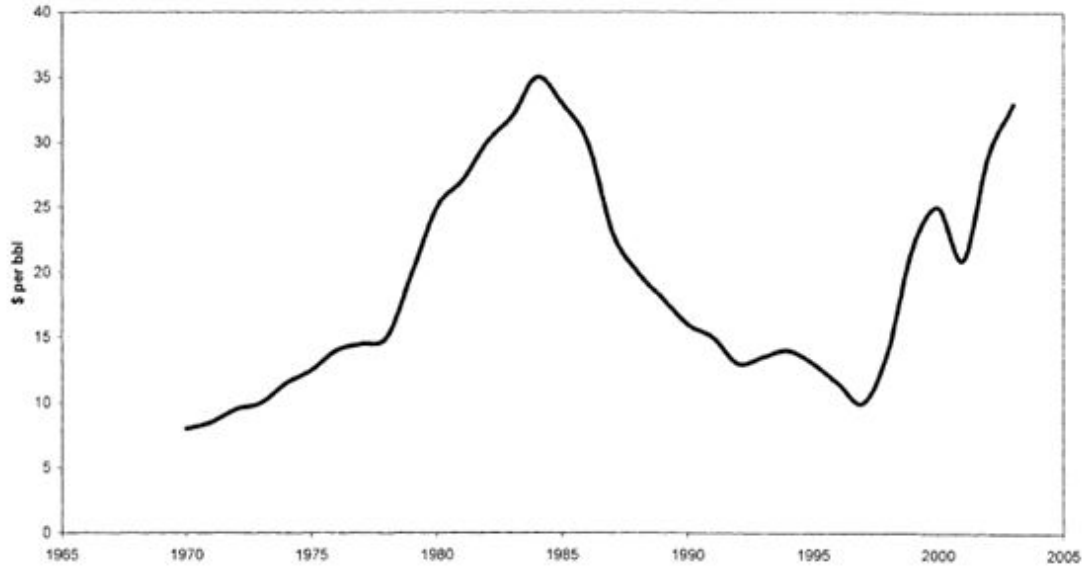

Figure 2.1. Crude oil price trend (Dry,2002)

Figure 2.2. Trend of oil price for the last 5 years (adapted from www.oil-price.net, 2010)

A number of reactions are involved in the Fischer-Tropsch synthesis. The product spectrum of FT synthesis includes linear and branched hydrocarbons and oxygenated products, however, linear paraffins and α-olefins are referred as main products of the synthesis (Van der Laan and Beenackers, 1999b). In case of CO decomposition on catalyst, Boudouard reaction, a side reaction to FT synthesis, may occur forming CO_2 and carbon (Dry, 2004). An outline of the reactions is given in Table 2.1.

The compositions of the hydrocarbon products of Fischer Tropsch synthesis show a distinctly regular pattern (Shulz, 1999). It was first noticed in 1946 by Herrington that the molar amount of individual carbon number fractions was to decline exponentially with carbon number, which was accepted to indicate similarity to polymerization kinetics (Schulz and Claeys, 1999; Yang *et al.*, 2003). It is agreed that -CH_2- is acting

Table 2.1. Reactions involved (Van der Laan and Beenackers, 1999b)

Main reactions	
1. Paraffins	$(2n + 1)H_2 + nCO \rightarrow C_nH_{2n+2} + nH_2O$
2. Olefins	$2nH_2 + nCO \rightarrow C_nH_{2n} + nH_2O$
3. Water Gas Shift reaction	$CO + H_2O \leftrightarrow CO_2 + H_2$
Side reactions	
4. Alcohols	$2nH_2 + nCO \rightarrow C_nH_{2n+2}O + (n\text{-}1)H_2O$
5. Boudouard reaction	$2CO \rightarrow C + CO_2$
Catalyst modifications	
6. Catalyst oxidation/reduction	a. $M_xO_y + yH_2 \leftrightarrow yH_2O + xM$
	b. $M_xO_y + yCO \leftrightarrow yCO_2 + xM$
7. Bulk carbide formation	$yC + xM \leftrightarrow M_xC_y$

as the monomer in FT synthesis and building blocks of hydrocarbons. It is then argued that there should be way to indicate the growth probability of chains just as in ideal polymerization reactions (Steynberg, 2004).

In most of the studies in literature, it is concluded that the hydrocarbon product composition of the Fischer-Tropsch synthesis follows the Anderson-Schulz-Flory (ASF) distribution. This distribution is defined by a term called growth probability, α, which shows the probability of the addition of a carbon intermediate to a chain. Growth probability depends on reaction conditions and type of catalyst used (Lox and Froment, 1993; Van der Laan and Beenackers, 1999a). ASF specifies growth probability as independent of the carbon number (Wang *et al.*, 2003). However, through experiment it is reported there are significant deviations from ASF distribution, such as high methane yield, anomalies of ethane and ethene productions as a result of secondary reactions, decrease in olefin to paraffin ratio. The deviations from ASF led researchers to search for new methods to predict the product distribution of FT synthesis (Van der Laan and Beenackers, 1999a).

FT synthesis involves the production of linear hydrocarbons, which directly affects

the quality of the diesel and the gasoline produced (Dry, 1999). The importance of this synthesis is that, since its aromaticity is low and sulphur, nitrogen or heavy metal content is zero, the fuel produced by Fischer-Tropsch synthesis is said to be of high quality. The high cetane number of the middle distillate fraction obtained, is the indicator of superior combustion properties and reduced emissions from burning of this fuel (Fox, 1993; Gregor, 1990; Steynberg, 2004). Transportation of fuel is one or may be the most important concept in industry. The Fischer-Tropsch synthesis diesel has unique advantages when compared to other fuels; it has high energy density, i.e. the energy stored per volume is greater. Moreover, its low vapor pressure dampens the safety issues related to the storage of FT diesel. Additionally, FT diesel is not soluble in water and it is biodegradable (Stenberg and Dry, 2004).

Fischer-Tropsch synthesis can be classified according to the range of the processing temperature, as high temperature Fischer-Tropsch (HTFT) with an approximate temperature range of 300-350°C, and low temperature Fischer-Tropsch (LTFT) with an approximate temperature range of 200-240°C (Dry, 2002). Primary product of HTFT is more branched and more olefinic than that of LTFT process. The Anderson-Schulz-Flory distribution of HTFT products is more towards lighter products in the range of gasoline and diesel fuel. LTFT primary products can be classified as two groups; hydrocarbon condensate forming the light fraction which is liquid at room conditions and a heavy fraction, known as wax, formed of heavy paraffins (Dancuart *et al.*, 2004; Dry and Steynberg, 2004). LTFT process enables the production of high quality diesel, with cetane number of approximately 75, in large amounts, whereas a large portion of the products in HTFT belongs to light alkenes. Additionally, the ratio of diesel to naphtha in the end product is higher in LTFT process revealing its superiority on HTFT process in diesel production. However, for production of gasoline, HTFT is a much better choice in terms of gasoline selectivity and octane number (Dry, 1999). To summarize, LTFT process is chosen if the main product is desired to be diesel and HTFT process is applied when preferred product is gasoline (Dry and Steynberg, 2004).

2.2.1. Catalysts for FT synthesis

Catalytic activity for FT reactions can only be provided with metals from group VIII, namely Fe, Co and Ru (Dry, 2002; Van der Laan and Beenackers, 1999b). Iron-based catalysts are commonly used because of their low costs in comparison to other metals active in FT synthesis (Van der Laan and Beenackers, 1999b). For iron-based catalysts high conversions, e.g. 90%, can be achieved but this requires two stage operation together with gas recycling and this increases both capital and running costs. The conversion profile does not change with an increase in total pressure if the residence time and other variables are constant. Thus, doubling the pressure and the gas feed rate results in doubling the reactor's production rate (Dry, 2002). Additionally, when using synthesis gas produced from coal, iron catalysts are better compared to cobalt-based catalyst in terms of enduring the possible poisoning (Steynberg, 2004).

There are many advantages of using cobalt-based catalyst. In FT synthesis, the highest yields hydrocarbons are obtained when using cobalt catalysts. Their lifetime is the longest and a large amount of the products are made up of linear alkanes when Co is used as catalyst. Additionally, as water does not have an inhibitive effect on Co catalysts, it is possible to achieve higher productivity at higher syngas conversions. However, since the activity of Co-based catalysts towards water gas shift (WGS) is low and they favor production of CH_4 in large amounts at high temperatures, their usage is mostly limited to LTFT processes (Dry, 2002; Van der Laan and Beenackers, 1999b). Also, FT reactions are more sensitive to H_2/CO ratio when using cobalt catalysts (Dry, 2004).

Ruthenium is another possible FT catalyst; it is very active but expensive compared to Co and Fe and it is not widely available (Dry, 2002; Van der Laan and Beenackers, 1999b). Therefore Ru-based catalysts are not used commercially.

2.2.2. Influence of Process Conditions on the Selectivity

FT synthesis results in a wide variety of products, i.e. alkanes, alkenes, alcohols and oxygenates with carbon numbers in the C_1-C_{20+} range. Selective distribution of these products is strongly related to the operating conditions, such as temperature, pressure and feed composition (Dry, 2002; Van der Laan and Beenackers, 1999b).

2.2.2.1. Temperature. Process temperature has much more significance on FT synthesis and product distribution than any other operating condition (Dry, 2002; Schulz, 1999; Van der Laan and Beenackers, 1999b). Running the reaction at high temperatures leads to a shift towards products with lower carbon numbers on each catalyst type, producing more of secondary products such as ketones and aromatics. More specifically, high temperature results in a distribution where light alkenes (C_2-C_7) and light alkanes (C_1-C_7) are higher in amount, and heavy alkenes (C_9-C_{26}) and heavy alkanes (C_{15+}) are lower. Thus, the average chain length of products decreases, but the branching increases. Additionally, selectivity of methane increases, as FT reaction mechanism favors methane production at high temperatures (Dry, 2002; Ji *et al.*, 2001; Schulz, 1999; Van der Laan and Beenackers, 1999b). In other words, carbon number of the products increase but this is caused by increased degree of branching as temperature reaches higher values (Dry, 2004). The ratio of produced alkenes to alkanes, i.e. olefin to paraffin ratio, also decreases with increasing temperature as conditions become suitable for hydrogenation to take place easily (Dry, 2004). High temperatures should also be avoided to prevent catalyst deactivation. Temperature increase results in carbon deposition on catalyst particles, which then lead to the deactivation of the catalyst, especially in the case of iron-based catalysts (Schulz, 1999; Steynberg, 2004).

Since FT reaction has a highly exothermic nature, control of temperature within the reactor system should be handled carefully. As the product quality is termed to be high because of longer chains with low degree of branching and low aromaticity content, inaccurate temperature control leads to deviations from this targeted product quality (Steynberg, 2004).

2.2.2.2. Total Pressure. Total pressure is another variable that affects product distribution in FT synthesis. It is shown that increase in total pressure results in shift in product selectivity towards heavier products and more oxygenates (Van der Laan and Beenackers, 1999b). It is also reported in literature that the percent conversion remains constant when the total pressure is increased while keeping other variables constant (Dry, 2002). In LTFT process, selectivity of hard wax, which is produced the most, is not affected by any change in pressure. However, in HTFT operations, increase in total pressure results in a shift to heavier products with a decrease in methane selectivity (Dry, 2004).

In a study of Mazonne and Fernandes (2006), which is oriented towards modelling FT synthesis over an iron based catalyst, results show that the total pressure does not show any significant influence on neither CO conversion nor hydrocarbon yield. With every 10 atm increase in the total pressure, only 2 to 15% increase in the hydrocarbon yield and decrease in CO conversion are observed. This is related to the fact that FT reaction rate is directly proportional to the total pressure. Also, the rate of water-gas shift (WGS) is not directly affected by the total pressure, but by the partial pressure of steam, which depends on the conversion level. Yield of light olefins is found to be strongly influenced by pressure. Increase in total pressure leads to a decrease in the amount of light olefins produced. Hence, total pressure of the system is claimed to be as important as any other factor in determining the amount of the desired product (Mazzone and Fernandes, 2006).

In another study, the growth probability is reported to be almost independent of the total pressure and the hydrogen partial pressure, but that it increases with increasing carbon monoxide partial pressure (Lox and Froment, 1993).

2.2.2.3. Feed composition (molar H_2/CO ratio). The importance of H_2/CO ratio arise from the fact that cost of syngas makes up a great amount of the capital and running cost. Thus, it is crucial to achieve the highest possible conversion in FT reactors. This requirement can be satisfied by using syngas with the correct composition, which

should be 2.0 (Dry, 2002; Dry, 2004).

As the molar H_2/CO ratio is increased, synthesis gas conversions become higher. This favors the production of steam and, thus facilitates the rate of the water-gas shift reaction. In such a case the CO conversions will be high, but the yields of heavier hydrocarbons will be adversely affected (Lu and Lee, 2007). In terms of the products, it can be said that an increase in this ratio results in lighter hydrocarbons and a lower olefin content (Donnelly and Satterfield, 1993; Dry, 2002). However, deficiency of hydrogen in feed leads to a loss in efficiency of the process since required hydrogen is produced from water molecules by spending energy for breaking the bonds (Steynberg, 2004).

It is shown that the lower H_2/CO ratio in feed favor the production of heavier alkenes (C_{9+}). It is noted that the lowest H_2/CO ratio in feed leads to the existence of a high amount of heavy alkenes up to about C_{26} (Ji *et al.*, 2001). The effect this ratio on type of products formed can be understood from Table 2.2, where H_2 to CO usage ratio stands for the H_2/CO ratio.

Table 2.2. Usage ratio of FT reactions (Dry, 2004)

FT product	Reactions	H_2 to CO usage ratio
CH_4	$3H_2 + CO \rightarrow CH_4 + H_2O$	3
C_2H_6	$5H_2 + 2CO \rightarrow C_2H_6 + 2H_2O$	2.5
Alkanes	$(2n + 1)H_2 + nCO \rightarrow C_nH_{2n+2} + nH_2O$	(2n+1)/n
Alkenes	$2nH_2 + nCO \rightarrow C_nH_{2n} + nH_2O$	2
Alcohols	$2nH_2 + nCO \rightarrow C_nH_{2n+1}OH + (n-1)H_2O$	2

H_2 is responsible for the termination of hydrocarbon chains into paraffins. Increasing H_2/CO ratio will increase partial pressure of H_2, also the termination rate into paraffins, reducing the amount of olefins produced. This indicates that at low H_2/CO ratios as H_2 amount will not be enough to produce high quantities of paraffins, olefin production fraction will be maximized (Dry, 2002; Lu and Lee, 2007). Probability of

chain termination increases when either partial pressure of CO is low or that of H_2 is high. Low partial pressure of CO decreases the surface coverage of CH_2- molecules, i.e. monomers, thus leads to chain termination. On the other hand, higher partial pressure of H_2 gives more opportunity for chain termination to occur by hydrogenation. Thus increasing H_2/CO ratio leads to higher methane selectivity and lighter products (Dry, 2004). As H_2/CO ratio in the syngas is increased, CO conversion and methane selectivity increase, paraffin-to-olefin ratio increases slightly, but selectivity of products over 5 carbons decreases (Lu and Lee, 2007).

Addition of CO_2 and H_2O is also another important parameter affecting the FT product distribution. Increasing the partial pressure of H_2O inhibits the FT reactions; especially with iron-based catalyst, since cobalt-based ones are not affected by water. Increasing partial pressure of CO_2 in the feed results in a decrease of methane selectivity (Van der Laan and Beenackers, 1999b). It is also stated that extra CO_2 causes water gas shift reaction to move in the reverse direction producing CO, which then is converted to hydrocarbons (Lu and Lee, 2007).

2.2.2.4. Space velocity. Increasing the space velocity results in an increase in olefin-to-paraffin ratio, thus leads to a decrease in conversion of syngas. This increase also leads to an increase in selectivity to methane and to olefins; however, selectivity towards paraffins is not much affected by the change in space velocity (Iglesia *et al.*, 1991; Kupiers *et al.*, 1996).

Production of alkenes (C_2-C_7) remains almost unchanged when space velocities are higher than 3,000 $h^{-}1$, while those of heavy alkenes (C_{8+}) increase. At low space velocities, the contents of alkenes larger than C_7 are significantly lower compared with those obtained at higher space velocities. With the increase of space velocity, alkene distributions over C_9-C_{15} gradually become horizontal. It is also found that C_1-C_{27} alkanes slightly decrease with the increase of space velocity, especially at low space velocity. For the alkanes above C_{27} the distributions become more complicated. Generally, the effect of space velocity on alkanes is less than on alkenes (Ji *et al.*, 2001).

3. MODELING AND SIMULATION OF THE MICROCHANNEL REACTOR SYSTEM

This chapter describes the microchannel reactor system and the methods used in its modeling and simulation. In this study, high temperature mode of Fischer-Tropsch (HTFT) synthesis over iron-based catalyst is selected due to the availability of kinetic data in the literature. The maximum carbon number is taken as 7 for ensuring that no condensation occurs in the microchannels, which allowed the construction of the model based on two phases - gas (fluid) and washcoat (catalyst); in simulations, the inlet temperature of feed to reaction is taken as 623 K (350°C) and the minimum temperature achieved in all simulations is approximately 600 K (327°C). Considering data in Table 3.1, it can be claimed that treating the stream in reaction channel completely as in gas phase is not wrong.

Table 3.1. The minimum reactor temperature required to avoid a liquid phase in various product cuts (Steynberg *et al.*, 2004)

Cut (by mass fraction)	Minimum temperature to avoid liquid condensation (°C)
C_2-C_5	109
C_5-C_{11}	329
C_5-C_{18}	392
C_{12}-C_{18}	468

In order to be sure that the mixture in reaction channel is completely in gas phase, another simulation is conducted using ChemCAD^{TM} process simulation software. In ChemCAD^{TM}, a mixture having the suitable compositions of products and reactants with reaction profile, is made to pass through a pipe having the same properties as the reaction channel. The result of this simulation, given in Table 3.2 verifies that liquid phase formation do not occur in the reaction channel.

Table 3.2. ChemCAD^{TM} result of stream properties in reaction channel

Temperature	623.15 K
Pressure	20 atm
Vapor mole fraction	1.0

Some simplifications have also been made in the reaction network. Olefin and paraffin producing reactions and water gas shift (WGS) reaction are treated as the only reactions taking place in microchannel, discarding any side reactions producing alcohols and ketones. The generalized form of the paraffin and olefin producing reactions and the WGS can be given as follows, where n is taken from 1 to 7 in this work:

Table 3.3. Involved reactions

Paraffins	$(2n + 1)H_2 + nCO \leftrightarrow C_nH_{2n+2} + nH_2O$	$(n \geq 1)$
Olefins	$2nH_2 + nCO \leftrightarrow C_nH_{2n} + nH_2O$	$(n \geq 2)$
Water Gas Shift	$CO + H_2O \leftrightarrow CO_2 + H_2$	

The exothermic nature of FT synthesis arises from the fact that the reaction enthalpy of paraffin reactions is -150 kJ per mole converted CO (Guettel *et al.*, 2008). WGS reaction, on the other hand, has the reaction enthalpy of -41.2 kJ/mol (Callagan, 2006).

3.1. Modelling

The microchannel reactor system, presented in Figure 3.1, is composed of reaction channels, which are coupled with cooling channels that serve as heat sinks to absorb the heat released from FT channels as a result of the exothermic reactions.

It can be observed from Figure 3.1 that system is comprised of square-shaped microchannels placed in a parallel configuration. Walls of reaction (FT synthesis) channels are considered to be coated with a porous, iron-based catalyst layer, forming the "washcoat" domain. Since, the properties of the fluids flowing within the channels

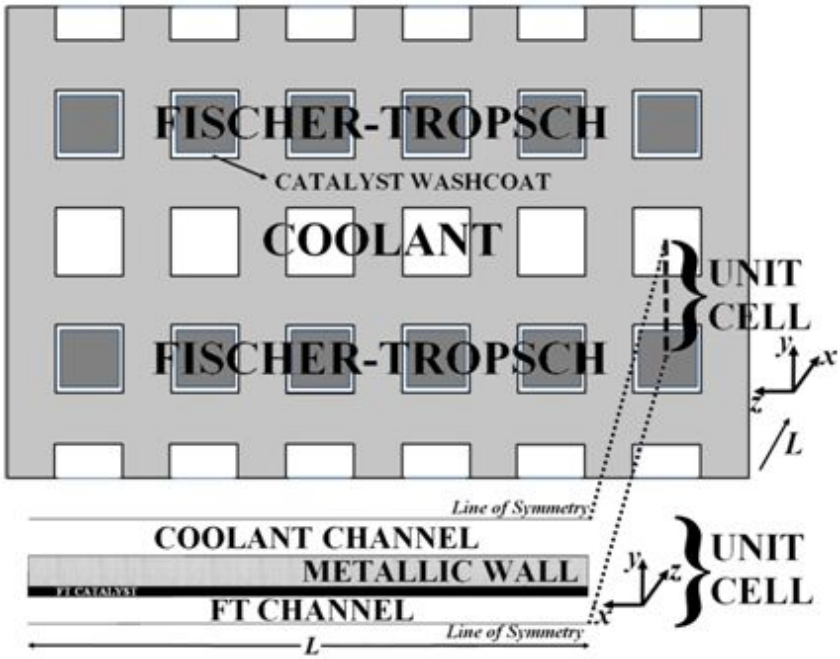

Figure 3.1. System configuration

of the same (horizontal) group do not differ, it is assumed that heat transfer between the channels of the same group (i.e. in z-direction) is negligible compared to heat flow between the channels of different groups (i.e. in y-direction). As the calculations are done in Cartesian coordinates, this means that in model equations, any kind of effect contributing from z-direction, according to Figure 3.1, is eliminated. Thus, the calculations are based on a two-dimensional unit cell, which is made up of the domain between the center lines of two channels through the channel length, as shown in Figure 3.1. The repeating pattern of the channels in the y-direction, and the resulting symmetry allows the consideration of the half-channel heights in the unit cell, which is the characteristic unit of the multichannel unit. In other words, behavior of the multichannel unit can be understood once the unit cell can be modeled and simulated. A detailed presentation of the unit cell is given in Figure 3.2.

Modeling of the simultaneous FT reaction and cooling in the unit cell configuration requires the consideration of equation of continuity together with momentum, energy and species mass conservation equations for the three domains, namely the fluid phase, catalytic washcoat phase and the solid, metallic wall phase. The reactor geometry is represented and the model equations are set using cartesian coordinates. It is

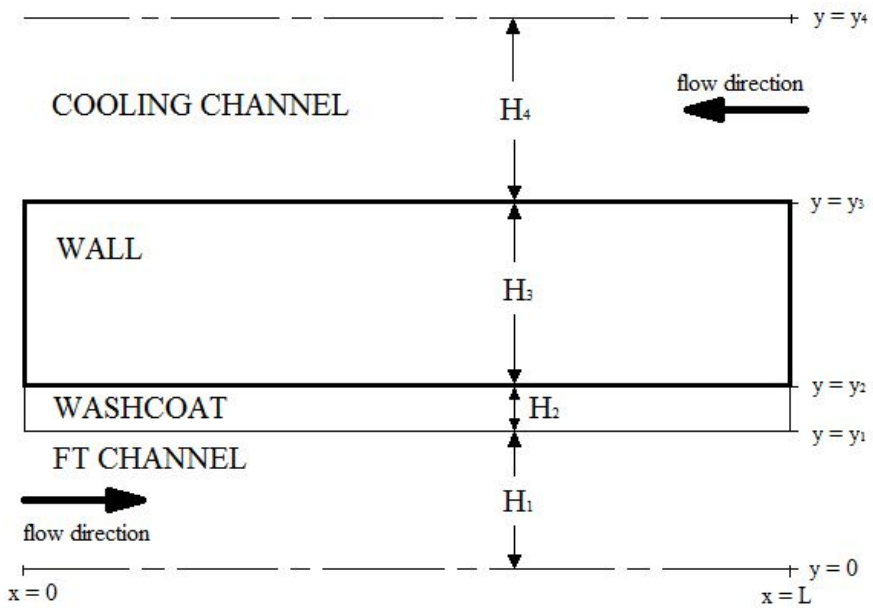

Figure 3.2. Unit cell of the microchannel reactor system

assumed that the reactions only occur in washcoat domain, i.e. there is no reaction taing place in fluid phase. That gases are assumed to be incompressible Newtonian fluids and they are treated as ideal gases. The main assumption is that coolant flow is present in cooling channels before reaction mixture is introduced into the system.

Conservation of momentum is valid in domains involving fluid flow. Therefore the relevant equations are composed for coolant and catalytic reaction (FT) channels. The two dimensional Navier-Stokes equations in cartesian coordinates for incompressible Newtonian fluids, used to solve for conservation of momentum in the fluid phase are given as follows (Bird *et al.*, 2007):

$$\rho_m \left(\upsilon_{x,m} \frac{\partial \upsilon_{x,m}}{\partial x} + \upsilon_{y,m} \frac{\partial \upsilon_{x,m}}{\partial y} \right) = -\frac{\partial p_m}{\partial x} + \mu_m \left(\frac{\partial^2 \upsilon_{x,m}}{\partial x^2} + \frac{\partial^2 \upsilon_{x,m}}{\partial y^2} \right) \tag{3.1}$$

$$\rho_m \left(\upsilon_{x,m} \frac{\partial \upsilon_{y,m}}{\partial x} + \upsilon_{y,m} \frac{\partial \upsilon_{y,m}}{\partial y} \right) = -\frac{\partial p_m}{\partial x} + \mu_m \left(\frac{\partial^2 \upsilon_{y,m}}{\partial x^2} + \frac{\partial^2 \upsilon_{y,m}}{\partial y^2} \right) \tag{3.2}$$

where m is used to identify the channel as FT channel (m =1) or cooling channel (m =2). Since washcoat is a porous texture, the form of momentum conservation equations known as Brinkman equations are used (Bird *et al.*, 2007):

$$\left(\frac{\mu_1}{\kappa}\right) \upsilon_{x,1} = -\frac{\partial p_1}{\partial x} + \left(\frac{1}{\varepsilon_p}\right) \mu_1 \left(\frac{\partial^2 \upsilon_{x,1}}{\partial x^2} + \frac{\partial^2 \upsilon_{x,1}}{\partial y^2}\right) \tag{3.3}$$

$$\left(\frac{\mu_1}{\kappa}\right) \upsilon_{y,1} = -\frac{\partial p_1}{\partial x} + \left(\frac{1}{\varepsilon_p}\right) \mu_1 \left(\frac{\partial^2 \upsilon_{y,1}}{\partial x^2} + \frac{\partial^2 \upsilon_{y,1}}{\partial y^2}\right) \tag{3.4}$$

In Equations (3.3) and (3.4), ε_p is the porosity and κ is the permeability related with the used catalyst. The porosity is taken as 0.5 (Shen *et al.*, 1996) and permeability as 1x10^{-8} (Avcı *et al.*, 2009). Boundary conditions related to Equations (3.1) to (3.4) are given in Table 3.4.

Table 3.4. Boundary conditions used for the momentum conservation equations

x=0	$0 < y < y_1$	$\upsilon_1=\upsilon_1^0$
	$y_3 < y < y_4$	$p_2 = p_{2out}$
x=L	$0 < y < y_1$	$p_1 = p_{1out}$
	$y_3 < y < y_4$	$\upsilon_2=\upsilon_2^0$
y=0	∀x	n.υ_1=0
y=y_1	∀x	n.υ_1=0
y=y_2	∀x	υ_1=0
y=y_3	∀x	υ_2=0
y=y_4	∀x	n.υ_2=0

In the FT channel, mass transport of species should also be calculated, since the concentration of reactants and products change along the channel and in the washcoat domain as a result of FT synthesis. On the fact that reactions only occur on catalytic

washcoat phase, the Equations (3.5) and (3.6) are used to calculate mass transfer in fluid passage and washcoat, respectively (Bird *et al.*, 2007).

$$\upsilon_{x,1}\frac{\partial c_A}{\partial x}+\upsilon_{y,1}\frac{\partial c_A}{\partial y}=\mathcal{D}_{AB}\left(\frac{\partial^2 c_A}{\partial x^2}+\frac{\partial^2 c_A}{\partial y^2}\right) \tag{3.5}$$

$$\upsilon_{x,1}\frac{\partial c_A}{\partial x}+\upsilon_{y,1}\frac{\partial c_A}{\partial y}=\mathcal{D}_{AB,eff}\left(\frac{\partial^2 c_A}{\partial x^2}+\frac{\partial^2 c_A}{\partial y^2}\right)+r_A \tag{3.6}$$

Note that subscript A is used to indicate the species CO, H_2, CO_2, CH_4, C_2H_4, C_2H_6, C_3H_6, C_3H_8, C_4H_8, C_4H_{10}, C_5H_{10}, C_5H_{12}, C_6H_{12}, C_6H_{14}, C_7H_{14}, C_7H_{16}. Boundary conditions related to Equations (3.5) and (3.6) are given in Table 3.5.

Table 3.5. Boundary conditions used in mass transport equations

x=0	$0 < y < y_1$	$c_A=c_A^0$
x=L	$0 < y < y_1$	$n.(-\mathcal{D}_{AB} \bigtriangledown c_A)=0$
y=0	$\forall x$	$n.(-\mathcal{D}_{AB} \bigtriangledown c_A+c_A \upsilon_1)=0$
$y=y_2$	$\forall x$	$n.(-\mathcal{D}_{AB} \bigtriangledown c_A+c_A \upsilon_1)=0$

Effective diffusivity appearing in Equation (3.6) is calculated from binary diffusivity by taking tortuosity, which is taken as 4 (Shen *et al.*, 1996), and porosity of the catalyst into account (Geankoplis, 2003):

$$\mathcal{D}_{AB,eff}=\frac{\varepsilon_A}{\tau}\mathcal{D}_{AB} \tag{3.7}$$

As the reactions take place, heat is released from FT channel due to the exothermic nature of the reactions. In order to control the reaction temperature, the fluid flowing in coolant channel is used to absorb the heat released from FT channel. The heat is generated in washcoat and dissipated into FT channel, reactor wall and coolant

channel. Such a heat transfer configuration can be modeled by using the equations given below. Equations 3.8, 3.9 and 3.10 give the temperature change in the fluid, washcoat and metallic wall phases, respectively (Bird *et al.*, 2007):

$$\rho_i C_{Pi} \left(\upsilon_{x,i} \frac{\partial T_i}{\partial x} + \upsilon_{y,i} \frac{\partial T_i}{\partial y} \right) = k_i \left(\frac{\partial^2 T_i}{\partial x^2} + \frac{\partial^2 T_i}{\partial y^2} \right) \tag{3.8}$$

$$\rho_i C_{Pi} \left(\upsilon_{x,i} \frac{\partial T_i}{\partial x} + \upsilon_{y,i} \frac{\partial T_i}{\partial y} \right) = Q + k_{eff} \left(\frac{\partial^2 T_i}{\partial x^2} + \frac{\partial^2 T_i}{\partial y^2} \right) \tag{3.9}$$

$$k_{wall} \left(\frac{\partial^2 T_i}{\partial x^2} + \frac{\partial^2 T_i}{\partial y^2} \right) = 0 \tag{3.10}$$

Boundary conditions related to Equations (3.8)-(3.10) are given in Table 3.6.

Table 3.6. Boundary conditions used in energy transport equations

x=0	$0 < y < y_1$	$T_1 = T_1^0$
	$y_1 < y < y_2$	n.$(-k_{eff} \bigtriangledown T_1)$=0
	$y_2 < y < y_3$	n.$(-k_{wall} \bigtriangledown T_w)$=0
	$y_3 < y < y_4$	n.$(-k_2 \bigtriangledown T_2)$=0
x=L	$0 < y < y_1$	n.$(-k_1 \bigtriangledown T_1)$=0
	$y_1 < y < y_2$	n.$(-k_{eff} \bigtriangledown T_1)$=0
	$y_2 < y < y_3$	n.$(-k_{wall} \bigtriangledown T_w)$=0
	$y_3 < y < y_4$	$T_1 = T_1^0$
y=0	∀x	n.$(-k_1 \bigtriangledown T_1)$=0
$y=y_1$	∀x	n.$(k_1 \bigtriangledown T_1 - k_{eff} \bigtriangledown T_1)$=0
$y=y_2$	∀x	n.$(k_{eff} \bigtriangledown T_1 - k_{wall} \bigtriangledown T_w)$=0
$y=y_3$	∀x	n.$(k_{wall} \bigtriangledown T_w - k_2 \bigtriangledown T_2)$=0
$y=y_4$	∀x	n.$(-k_2 \bigtriangledown T_2)$=0

In Equation (3.9), thermal conductivity of the washcoat domain is taken as 4.5 times of the thermal conductivity of the fluid (Avcı *et al.*, 2009).

The heat generated (Q) in catalyst layer as a result of reactions is calculated via molar enthalpies of species involved in reactions. The molar enthalpy of species A, ΔH_A (J mol^{-1}), at a specified temperature is calculated using Equation (3.11) (Smith *et al.*, 2005).

$$\Delta H_A = \Delta H_{A0} + R \int_{T_0}^{T} \frac{\Delta C_{PA}}{R}\, dT \tag{3.11}$$

The last term in Equation (3.11) is calculated by Equation (3.12) using constants γ, δ, ξ, φ related to the specific heat capacity, C_P (J mol^{-1} K^{-1}), calculation of species (Smith *et al.*, 2005).

$$\int_{T_0}^{T} \frac{\Delta C_{PA}}{R}\, dT = \gamma T_0(\tau - 1) + \frac{\delta}{2} T_0^2(\tau^2 - 1) + \frac{\xi}{3} T_0^3(\tau^3 - 1) + \frac{\varphi}{T_0}\left(\frac{\tau - 1}{\tau}\right) \tag{3.12}$$

where

$$\tau \equiv \frac{T}{T_0} \tag{3.13}$$

Generated heat term is calculated via Equation (3.14);

$$Q = \sum r_i \left(\sum \sigma_j \Delta H_j\right)_{rxn,i} \tag{3.14}$$

Finally, the continuity equation used in all channels and washcoat domain can be given as follows (Bird *et al.*, 2007):

$$\frac{\partial v_x}{\partial x} + \frac{\partial v_y}{\partial y} = 0 \tag{3.15}$$

Properties of solids (density, thermal conductivity) are assumed to be constant against temperature changes, whereas properties of gases are considered to change with temperature. Coolant is assumed to be a pure stream of steam, methane or air. Viscosity, thermal conductivity, heat capacity and density of pure gases are calculated using the following correlations (Crane Co., 1982; Sinnot, 2003; Smith *et al.*, 2005):

$$\mu = \mu_0 \left(\frac{T}{T_0}\right)^{3/2} \left(\frac{T_0 + S}{T + S}\right) \tag{3.16}$$

$$k = \mu \left(C_p + \frac{10.4}{M}\right) \tag{3.17}$$

$$C_p = R(\gamma + \delta T + \xi T^2 + \varphi T^{-2}) \tag{3.18}$$

$$\rho = \frac{PMw}{RT} \tag{3.19}$$

Since the kinetic expression used in this study predicts low conversion synthesis gas conversion levels (below ca. 10%) in the FT channel, it is assumed that the fluid mixture in the FT channel can be characterized by CO and H_2, and that their compositions remain almost constant. Physical and thermo-chemical properties of the reaction stream is calculated using the following mixing rules (Krieger, 1951; Sinnot, 2003):

$$\mu_{mix} = \sum_{i=1}^{q} \frac{\mu_i}{1 + \frac{1}{x_i} \sum\limits_{\substack{j=1 \\ j \neq i}}^{j=q} \frac{x_j [1+(\mu_i/\mu_j)^{1/2}(M_j/M_i)^{1/4}]^2}{2\sqrt{2}(1+(M_j/M_i)^{1/2})}} \tag{3.20}$$

$$k_{mix} = k_1 w_1 + k_2 w_2 \tag{3.21}$$

In Equation (3.20), q stands for the total number of species present in mixture, and is 2 for this case. Indexes i and j are used to designate CO (1) and H_2 (2) while calculating viscosity of the mixture.

$$C_{p_{mix}} = C_{p_1} x_1 + C_{p_2} x_2 \tag{3.22}$$

Binary diffusivity can be calculated using the following correlation (Poling *et al.*, 2004):

$$\mathcal{D}_{AB} = \frac{0.00143 T^{1.35}}{P M_{AB}^{0.5} [(\sum \vartheta)_A^{1/3} + (\sum \vartheta)_B^{1/3}]^2} \tag{3.23}$$

$$M_{AB} = 2 \left[\frac{1}{M_A} + \frac{1}{M_B} \right]^{-1} \tag{3.24}$$

The kinetic expressions of Langmuir-Hinshelwood type that are used for describing the rate of FT synthesis over a Fe-Cu-K catalyst are taken from Wang *et al.* (2003). They also proposed chain growth probabilities to be used with these rate expressions, which differ from the ASF probability in terms of taking the observed deviations from

the ASF distribution into account. The kinetic expressions involve separate terms for rates of formation of CH_4, C_{2+} alkanes and alkenes, and for WGS that runs as a side reaction. Rate of formation of methane is given by the following expression:

$$R_{CH_4} = \frac{k_{5M} P_{H_2} \alpha_1}{1 + \left(1 + \frac{1}{K_2 K_3 K_4} \frac{P_{H_2O}}{P_{H_2}^2} + \frac{1}{K_3 K_4} \frac{1}{P_{H_2}} + \frac{1}{K_4}\right) \sum_{i=1}^{N} \left(\prod_{j=1}^{i} \alpha_j\right)} \tag{3.25}$$

For olefins and paraffins, where carbon number is greater or equal to 2, following expressions are proposed:

$$R_{C_n H_{2n+2}} = \frac{k_5 P_{H_2} \prod_{j=1}^{n} \alpha_j}{1 + \left(1 + \frac{1}{K_2 K_3 K_4} \frac{P_{H_2O}}{P_{H_2}^2} + \frac{1}{K_3 K_4} \frac{1}{P_{H_2}} + \frac{1}{K_4}\right) \sum_{i=1}^{N} \left(\prod_{j=1}^{i} \alpha_j\right)} \tag{3.26}$$

$$R_{C_n H_{2n}} = \frac{k_6 (1 - \beta_n) \prod_{j=1}^{n} \alpha_j}{1 + \left(1 + \frac{1}{K_2 K_3 K_4} \frac{P_{H_2O}}{P_{H_2}^2} + \frac{1}{K_3 K_4} \frac{1}{P_{H_2}} + \frac{1}{K_4}\right) \sum_{i=1}^{N} \left(\prod_{j=1}^{i} \alpha_j\right)} \tag{3.27}$$

For the water-gas shift reaction, rate of carbon dioxide formed is given as follows:

$$R_{CO_2} = \frac{k_v (P_{CO} P_{H_2O} / P_{H_2}^{0.5} - P_{CO_2} P_{H_2}^{0.5} / K_P)}{1 + K_v P_{CO} P_{H_2O} / P_{H_2}^{0.5}} \tag{3.28}$$

The terms, α and β, stand for the growth probability and are given using the following expressions:

For n=1;

$$\alpha_1 = \frac{k_1 P_{CO}}{k_1 P_{CO} + k_{5M} P_{H_2}} \tag{3.29}$$

For n≥2;

$$\alpha_n = \frac{k_1 P_{CO}}{k_1 P_{CO} + k_5 P_{H_2} + k_6(1-\beta_n)} \tag{3.30}$$

For Anderson-Schulz-Flory growth probability;

$$\alpha_A = \frac{k_1 P_{CO}}{k_1 P_{CO} + k_5 P_{H_2} + k_6} \tag{3.31}$$

For n≥2;

$$\beta_n = \frac{k_{-6}}{k_6} \frac{P_{C_n H_{2n}}}{\alpha_A^{n-1} \frac{k_1 P_{CO}}{k_1 P_{CO} + k_5 P_{H_2}} + \frac{k_{-6}}{k_1 P_{CO} + k_5 P_{H_2} + k_6} \sum_{i=2}^{n} (\alpha_A^{i-2} P_{C_{(n-i+2)} H_{2(n-i+2)}})} \tag{3.32}$$

Rate constants are calculated using the expressions given as:

$$k_i(T) = k_{i,0} \exp(-E_i/RT) \tag{3.33}$$

Values of the constants that appear in Equations (3.25)-(3.33) are presented in Table 3.7.

Table 3.7. Rate expression parameters (Wang *et al.*, 2003)

Parameter	Dimension	Value
k_1	mol g^{-1} s^{-1} bar^{-1}	2.23 10^{-5}
$k_{5M,0}$	mol g^{-1} s^{-1} bar^{-1}	4.65 10^{3}
E_{5M}	kJ mol^{-1}	92.89
$k_{5,0}$	mol g^{-1} s^{-1} bar^{-1}	2.74 10^{2}
E_5	kJ mol^{-1}	87.01
$k_{6,0}$	mol g^{-1} s^{-1}	2.66 10^{6}
E_6	kJ mol^{-1}	111.04
$k_{v,0}$	mol g^{-1} s^{-1} $bar^{-1.5}$	1.57 10^{1}
E_v	kJ mol^{-1}	45.08
k_{-6}	mol g^{-1} s^{-1} bar^{-1}	1.13 10^{-3}
K_v	$bar^{-0.5}$	1.13 10^{-3}
K_2	-	1.81 10^{-2}
K_3	-	4.68 10^{-2}
K_4	-	0.226

In order to test the rate expressions, they are implemented into 1-D pseudo-homogeneous tubular reactor model which works under COMSOL Reaction Engineering Lab^{TM}. In Reaction Engineering Lab, concentration and temperature gradients are allowed only to develop in the axial direction. The species mass balances are given by (Fogler, 2006):

$$\frac{dF_i}{dV} = R_i \tag{3.34}$$

In Equation (3.34), V designates the volume of the reactor channel. Adiabatic operation is required to observe the temperature profile of the system. The energy equation deployed in calculations can be given as (Fogler, 2006):

$$\frac{dT}{dV} = \frac{\sum_{i=1}(-R_i)[-\Delta H_{rxn,i}(T)]}{\sum_{i=1} F_i C_{P_i}} \tag{3.35}$$

Solution of the model equations is performed using the COMSOL Multiphysics^{TM} package. COMSOL uses finite element method (FEM) to solve the partial differential equations. Stationary solver type is used since the solution is aimed to be achieved when the system approaches steady state. Whether to use a linear or non-linear solver is automatically decided by COMSOL with an analysis of the residual and the constraint Jacobian matrices. Damped Newton method is used to find the starting value of next iterative step. Solution is always carried out using linear systems, thus, non-linear systems are linearized before the solution. For linear systems, direct PARDISO solver is chosen, which uses Gaussian elimination method just as any direct solvers but requires less memory. Unstructured meshing is used with approximately 41,500 triangular elements in each solution.

In order to execute the solution, COMSOL requires initial temperature and total pressure of the system, inlet linear velocity to the channel and, for reaction channel only, initial compositions of species. Among these, composition values should be calculated to find the corresponding values at the specified operational conditions of the system. As temperature and pressure of the feed is fixed and the molar fractions of the species are known, the concentrations (mol/ m^3) in feed stream are calculated by Equation (3.35) (Fogler, 2006).

$$c_{A0} = \frac{P_{A0}}{RT_0} = \frac{y_{A0}P_0}{RT_0} \tag{3.36}$$

As inlet linear velocity and the geometry of the channel are known, the volumetric flow of feed, and the inlet molar flow of species can be calculated.

$$F_{A0} = c_{A0} V_0 \tag{3.37}$$

The outlet concentration and molar flows are given at their average values via integration over the boundaries as follows:

$$\bar{v}_1 = \frac{\int v_1 dS}{\int dS} \tag{3.38}$$

$$\bar{c}_A = \frac{\int c_A v_1 dS}{\int v_1 dS} \tag{3.39}$$

$$\bar{F}_A = \bar{c}_A \bar{v}_1 S \tag{3.40}$$

Partial pressures of species are required for calculating the rate of reactions. At any point within the reaction channel, partial pressures are calculated by ideal gas assumption.

$$P_A = c_A RT \tag{3.41}$$

Average temperature within the channel is calculated by integrating the temperature values at center line over the channel length and dividing this value to the channel length.

$$\bar{T} = \frac{\int T dL}{\int dL} \tag{3.42}$$

In order to discuss the results of the simulations, some parameters such as thermal conductivity (k), heat transfer coefficient (h), thermal diffusivity (α) of gases in both channels, and conduction parameter (λ) of the metallic wall between channels need to be calculated. Estimation of heat transfer coefficient for gases requires the prediction of Nusselt (Nu) number. Although in literature it is stated that Nu reaches a constant number in microchannels (Lee *et al.*, 2005; Enright *et al.*, 2006), a calcualtion procedure is required to find that constant value of Nu for the system used in this work. The following correlation is used to calculate the Nusselt number in the laminar flow regime (Bird *et al.*, 2007):

$$Nu = 1.86 \left(RePr \frac{D}{L} \right)^{1/3} \left(\frac{\mu_b}{\mu_0} \right)^{0.14} \tag{3.43}$$

In Equation (3.42), D (m) is the hydraulic diameter of the channel and L (m) is the channel length. μ_b and μ_0 stand for viscosity at the average bulk temperature and the average wall temperature, respectively. However, average bulk and wall temperatures do not differ significantly due to the presence of small dimensions. Therefore the 'wall correction' term involving the ratio of viscosities in Equation (3.42) can be neglected. The dimensionless numbers showing up in Equation (3.42), which are Re and Pr, are given explicitly as follows:

$$Re = \frac{\rho \upsilon d}{\mu} \tag{3.44}$$

$$Pr = \frac{C_p \mu}{k} \tag{3.45}$$

Having calculated Nusselt number, the heat transfer coefficient is calculated via

Equation (3.45).

$$h = \frac{Nuk}{D} \tag{3.46}$$

Thermal diffusivity, α, is defined as the ratio of heat conducted through the material to heat stored per unit volume (Incropera *et al.*, 2007).

$$\alpha = \frac{k}{C_p \rho} \tag{3.47}$$

Conduction parameter enables the comparison of significance of conduction heat transfer versus energy carried by the fluid (Peterson, 1999). A_c (m^2) term in conduction parameter equation, designates the cross section of the wall.

$$\lambda = \frac{k_{wall} A_c}{\dot{m} C_p L} \tag{3.48}$$

3.2. Parameters analyzed during simulations

The reaction mixture and coolant gases carry the properties given in Table 3.8 at the inlet of the channels for almost all simulations. Any change in these properties is given in the corresponding subsection.

Feed properties of the reaction mixture and coolant gases are given in Table 3.8. Inlet temperature of reaction mixture is chosen as the upper limit of HTFT synthesis, i.e. 350°C (623 K). After a literature survey based on experimental studies, it is observed that the volumetric flow rate is varied between 4x10^{-7} - 3.9x10^{-6} m^3/s STP in microchannels (Keyser et.al, 2004; Visconti, et.al, 2007). These values correspond to linear velocities of 1.5 - 15.5 m/s for the microchannel geometry selected in the present

work. Thus, linear velocities of both fluids are chosen as 5 m/s. Steam is selected as coolant in the default case, and its inlet temperature is taken as 374 K at 1 atm to make sure that no condensation occurs in the coolant side of the unit cell.

Table 3.8. Default properties of the feed streams

Reaction channel inlet flow	5 m/s
CO inlet molar flow rate	1.62 10^{-4} mol/s
H_2 inlet molar flow rate	3.24 10^{-4} mol/s
Molar H_2/CO ratio	2
Reaction inlet temperature	623 K
Reaction channel pressure	20 atm
Cooling inlet flow	5 m/s
Cooling inlet temperature	374 K
Cooling channel pressure	1 atm

Default dimensions and properties of the unit cell shown in Figure 3.2, are summarized in Table 3.9. Changes in these parameters in the context of parametric analyses are described in the corresponding subsections.

Table 3.9. Default properties of the unit cell

Side length of the reaction channel	500 μm	2xH_1
Washcoat thickness	50 μm	H_2
Reactor wall thickness	300 μm	H_3
Side length of the coolant channel	600 μm	2xH_4
Length	0.2 m	L
Reactor wall material	Steel-AISI	
Coolant	Steam	

3.2.1. Reactor wall thickness

Thickness of the wall separating the channels is changed to see its impact on heat transfer between channels and efficiency in providing isothermal operational conditions for reaction channel. Thickness is varied between 200 μm and 600 μm, while every other variable (wall material, channel side lengths, coolant type, inlet flows and conditions) is kept constant. The thickness values studied are: 200 μm, 300 μm, 400 μm, 500 μm and 600 μm.

3.2.2. Reactor wall material

Material of the wall separating the channels is changed to see the effect of wall conductivity on heat transfer between channels and efficiency in providing isothermal operational conditions for reaction channel. Wall material is changed, while every other variable (wall thickness, channel side lengths, coolant type, inlet flows and conditions) is kept constant. The change in material is actually the change in wall thermal conductivity. Possible materials of construction and their thermal conductivities are given in Table 3.10.

Table 3.10. Thermal conductivity of the materials of construction of the microchannel reactor

Material	Thermal conductivity k, W/(m.K)
Alumina (Al_2O_3)	27
AISI Steel	44.5
Aluminum	201
Copper	400

3.2.3. Coolant

Coolant is important in enabling isothermal conditions in reaction channel as its main role is to absorb the heat released form reaction channel. Thus, it is important to observe how system responds to different coolants, i.e. different fluids with different thermophysical properties, in other words with different capabilities to absorb heat in different amounts. In addition to steam, air and methane are selected as coolants. Since the aim is to observe the response to change of only one variable, inlet conditions and amount of the coolant is kept same for all simulations. Feed conditions, wall thickness, wall material and channel side lengths are also kept constant, i.e. used at their default settings (Tables 3.8 and 3.9).

3.2.4. Cooling Channel Side Length

Heat transfer coefficient is calculated from Nusselt number as shown in Equation (3.43). In microchannels, as a result of laminar flow, Nusselt number reaches a constant value (Lee *et al.*, 2005; Enright *et al.*, 2006). Hence, side length of the channel can be changed to enhance the heat transfer coefficient of the fluid (Steinke and Kandlikar, 2004).

Changing the diameter, i.e. the side length of the channel triggers other changes in the system, which may lead to missing some important points while discussing the results. Decreasing or increasing the side length will lead to a decrease or increase in the value of Re and mass flow rate, as long as the linear velocity is kept constant. However, Re and mass flow rate cannot be kept constant at the same time, so these are investigated as different cases.

3.2.4.1. Case I: Constant mass flow rate . In this case mass flow rate is taken as 1 10^{-6} kg/s , the default case value and the side length of the cooling channel varied as 400 μm, 500 μm, 600 μm and 700 μm. Corresponding linear velocities used are calculated and presented in Table 3.11.

Table 3.11. Linear velocities for constant mass flow in different side lengths

Side length (μm)	Linear velocity (m/s)
400	11.3
500	7.2
600	5.0
700	3.7

3.2.4.2. Case II: Constant Re . Reynolds number, which is calculated for the default case as 44.5, is taken as constant in this simulation. The side length of the cooling channel varied as 400 μm, 500 μm, 600 μm and 700 μm, as it is done in Case I. Corresponding linear velocities used are calculated and presented in Table 3.12.

Table 3.12. Linear velocities for constant Re in different side lengths

Side length (μm)	Linear velocity (m/s)
400	7.5
500	6.0
600	5.0
700	4.3

3.2.4.3. Case III: Constant linear velocity . Keeping linear velocity constant results in change in mass flow rate of the coolant as side length is changed. This simulation does not provide a discussion which is solely dependent on the change of mass flow rate; however, it will be helpful in understanding the response of the system to the change in side length. The side length of the channel, again, varied as 400 μm, 500 μm, 600 μm and 700 μm and the default linear velocity is taken as 5 m/s value. Corresponding mass flows rates can be found in Table 3.13.

3.2.5. Coolant mass flow rate

Case III of previous simulation does not provide the opportunity to investigate the possible effects of increasing/decreasing mass flow of coolant on the system. For

Table 3.13. Mass flow rates for constant linear velocity in different side lengths

Side length (μm)	Mass flow (kg/s) x10^6
400	0.5
500	0.7
600	1.0
700	1.4

this purpose, linear velocity of the coolant (steam) is changed 5 m/s, 10 m/s, 15 m/s and 20 m/s, while the other system properties constant as given in Tables 3.8 and 3.9. Corresponding mass flows of steam in each case are shown in Table 3.14.

Table 3.14. Mass flow rates

Linear velocity (m/s)	Mass flow (kg/s) x10^6
5	1.0
10	2.1
15	3.1
20	4.2

3.2.6. H_2/CO ratio

As mentioned in previous chapter, H_2/CO ratio is one of the most important factors that affect the FT synthesis significantly in terms of product spectra. This change results in different amounts of heat to be released. Hence, temperature profile within the channels is affected with this change.

The H_2/CO ratios for the parametric study are 1.5, 2 and 2.5. Inlet conditions of the streams and the flow rate of steam are kept as the same with default values (Table 3.8). However, the molar flow rates, thereby mass flows of H_2 and CO do change. Since temperature and pressure of the feed stream is taken as their default values (Table 3.8), total amount of moles that can be present in a specific volume is fixed. Thus, it is not possible to keep the amount of one specie constant and change the other one. As a

result, the total amount is distributed between H_2 and CO according the specified ratio. The ratios and the corresponding molar flows of H_2 and CO are given in Table 3.15.

Table 3.15. Molar flow rates of feed components for different H_2/CO ratios

H_2/CO ratio	H_2 molar flow (mol/s) x10^6	CO molar flow (mol/s) x10^6
1.5	2.89	1.92
2.0	3.24	1.62
2.5	3.42	1.37

3.2.7. Channel Property

In section 3.2.4, it is mentioned that the channel side length is expected to be one of the parameters that can affect temperature profiles. In addition to channel side length, in literature, property of the channel can also be important about the temperature distribution within the unit cell (Steinke and Kandlikar, 2004).

The micro baffles on the channel walls are used to implement different channel wall textures. Four different types of baffle designs are studied; their presence are simulated at the default values of the system properties given in Table 3.8. The dimensions and locations of the micro-baffles are presented in Table 3.16.

Table 3.16. Dimensions and location of the micro-baffles

Type	Width (m) x10^3	Length (m) x10^3	Location
I	5	0.15	Rxn channel
II	5	0.15	Both channels
III	5	0.15	Cooling channel
IV	10	0.15	Rxn channel

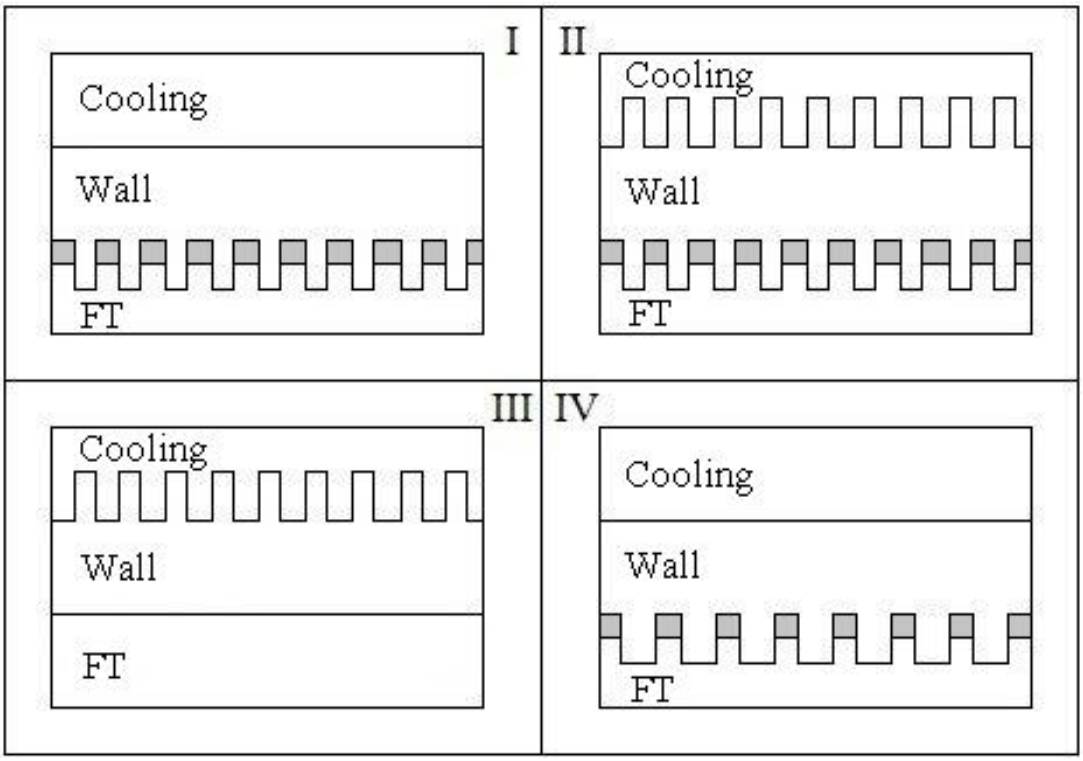

Figure 3.3. Micro-baffle geometries of Type I, II, III and IV

4. RESULTS AND DISCUSSION

The reaction mechanism of Fischer Tropsh synthesis is simulated using COMSOL Reaction Engineering Lab package and the parametric analysis of system defined in the previous chapter is carried out using COMSOL Multiphysics^{TM} package. The simulations are done for the systems in which the highest carbon number in product spectra is 3 (3C) and 7 (7C), with all hydrocarbons being linear alkanes and alkenes. The hydrocarbons in 3C case are CH_4, C_2H_4, C_3H_6, C_2H_6 and C_3H_8, while the hydrocarbons are CH_4, C_2H_4, C_3H_6, C_4H_8, C_5H_{10}, C_6H_{12}, C_7H_{14}, C_2H_6, C_3H_8, C_4H_{10}, C_5H_{12}, C_6H_{14} and C_7H_{16} in the 7C case. Apart from the hydrocarbons and unreacted CO and H_2, and CO_2 and H_2O, products of water-gas shift reaction, are present in the channel.

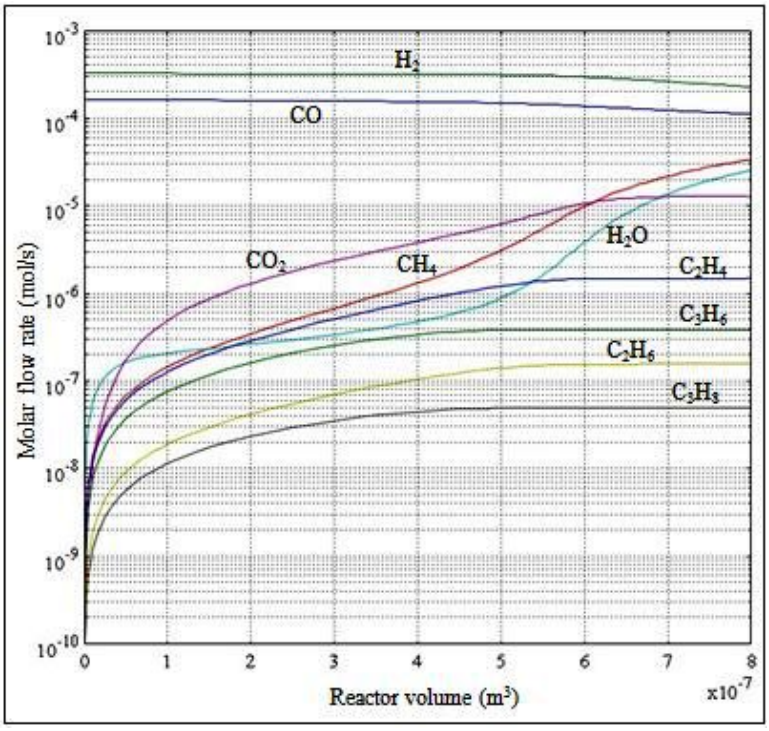

Figure 4.1. Molar flow rate profiles for the 3C case (inlet conditions: 535 K, 10 atm)

It is important to understand the nature of a reaction/combination of reactions before starting any further calculations based on that/these reaction(s). For this purpose, FT reactions (Table 3.3) are simulated in COMSOL Reaction Engineering Lab in the context of an adiabatic operation. In this work, it is aimed to control the temperature rise related to the heat generated in reaction channel, so it is important to see the

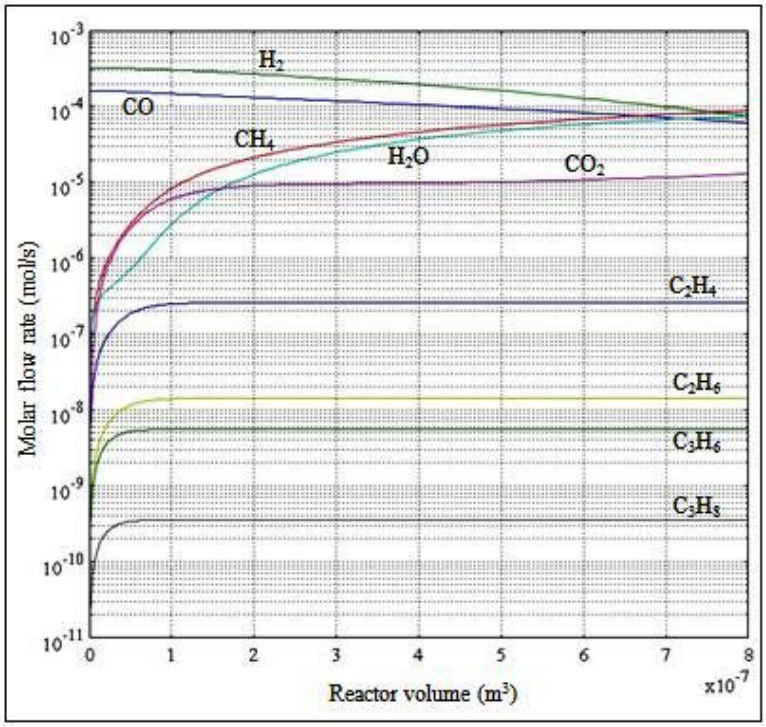

Figure 4.2. Molar flow rate profiles for the 3C case (inlet conditions: 623 K, 10 atm)

profile of FT synthesis in adiabatic system for to have an idea about an uncontrolled system. The reaction profile for adiabatic case is obtained as in Figure 4.1 for 3C case involving inlet temperature of 535 K and pressure of 10 atm.

The actual volume of the FT channel is $5x10^{-8}$ m^3. Considering this volume, it can be observed that the extents of the reactions are too low when the reactants are fed at 535 K. Therefore, a higher inlet temperature, 623 K, is tried to increase conversions of CO and H_2 in the catalytic microchannel, and the results are presented in Figure 4.2.

As can be observed from Figure 4.2, conversions of CO and H_2 are higher compared to the case of 535 K. Since 623 K is the upper limit of HTFT operation, further modification in the feed conditions to achieve a little higher conversion in actual volume is done by changing the inlet total pressure. Consequently, inlet conditions are set as 623 K and 20 atm and the resulting molar flow rate profiles are presented in Figure 4.3. It is found that the amount of hydrocarbons produced except methane, is very low. H_2 and CO leave the reactor at a lower value compared to the results in Figure

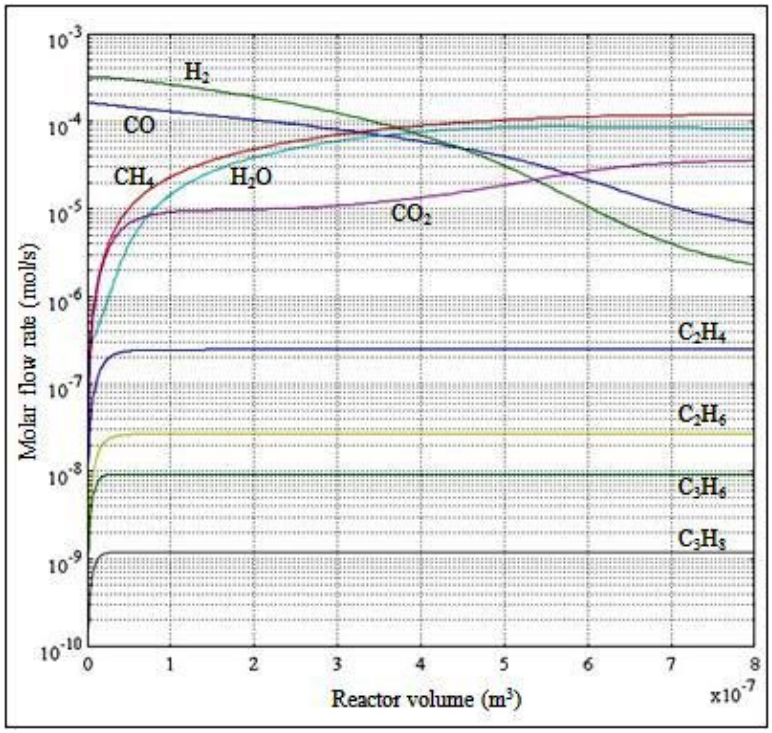

Figure 4.3. Molar flow rate profiles for the 3C case (inlet conditions: 623 K, 20 atm)

4.1, indicating that a higher conversion level, in comparison with the previous case, is obtained.

Temperature rise of the reaction channel for 3C case, if not controlled, i.e. run at adiabatic conditions can be observed in Figure 4.4. If figures 4.1 and 4.2 are examined together, it is clearly seen that, methane and temperature exhibit similar trends. As stated in literature, temperature rise favors methane production, thus, as temperature reaches 2300 K, it is expected that methane will be produced in large amounts compared to other hydrocarbons (Dry, 2002; Ji et al., 2001; Schulz, 1999; Van der Laan and Beenackers, 1999b).

After predicting the evolution of species molar flow rates and temperature for the 3C case, it is aimed to see the trends in the case of production of higher hydrocarbons. For this purpose, a seven-carbon (7C) case has been simulated under adiabatic conditions using identical feed properties (623 K, 20 atm). Molar flow rate and temperature profiles of the 7C case are presented in Figures 4.5 and 4.6, respectively.

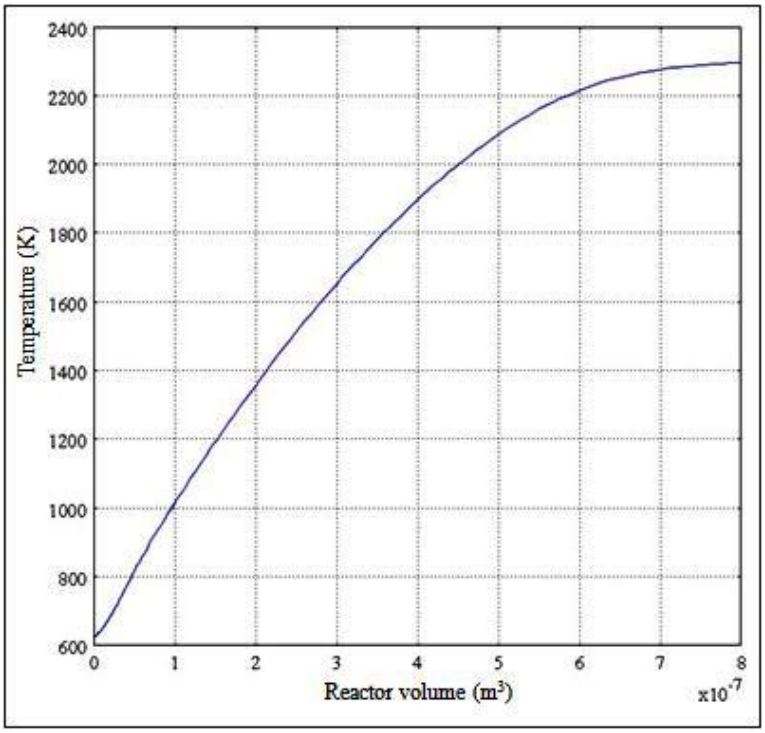

Figure 4.4. Temperature profile for the 3C case (inlet conditions: 623 K, 20 atm)

Since the flow amounts of produced hydrocarbons which are not included in 3C system are small, their effect on temperature profile is not significant to be clearly observed from Figure 4.6.

The temperature profiles obtained above clearly shows the necessity of temperature control in the FT reaction. In this work, it is aimed to provide temperature control in the parallel microchannel geometry presented in Section 3.1. The sections below include the results of the simulations conducted in COMSOL Multiphysics^{TM} and give the impact of particular geometric and operating parameters on the temperature evolution of the microchannels. The numerical results and profiles presented in the following sections are based on the values at the centerline of the channel.

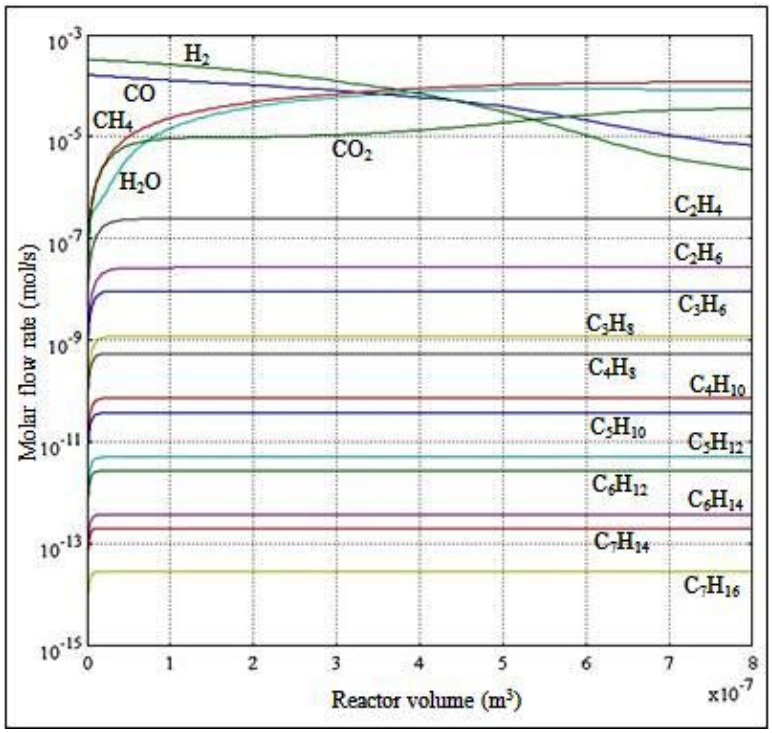

Figure 4.5. Molar flow rate profiles for the 7C case (inlet conditions: 623 K, 20 atm)

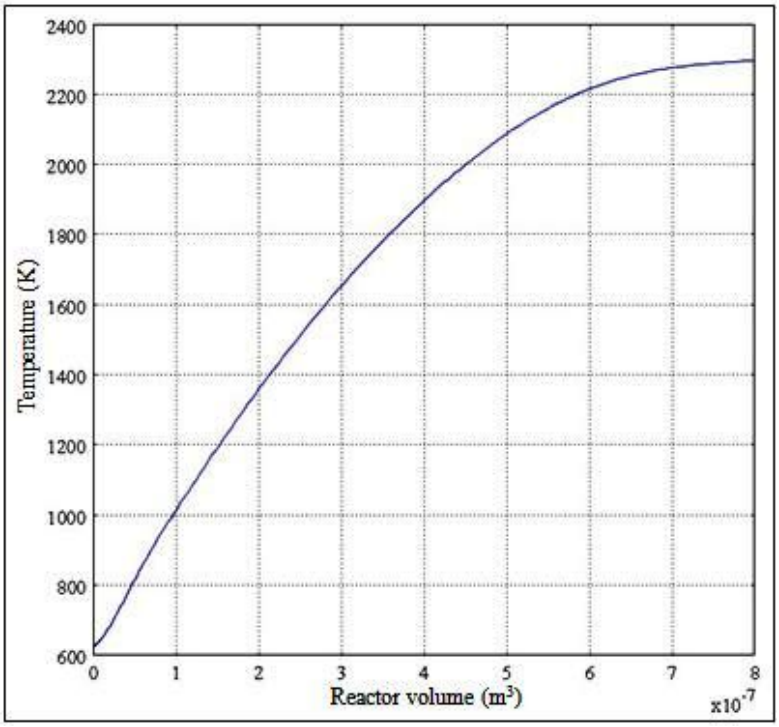

Figure 4.6. Temperature profile for the 7C case (inlet conditions: 623 K, 20 atm)

4.1. Effect of reactor wall thickness

Temperature profiles of the FT channel, obtained with different wall thickness values, are given in Fig. 4.7. It is observed that the maximum temperature in the reaction channel increases as the wall thickness decreases. It is also can be seen in Table 4.2 that the average temperature decreases with the increase in wall thickness.

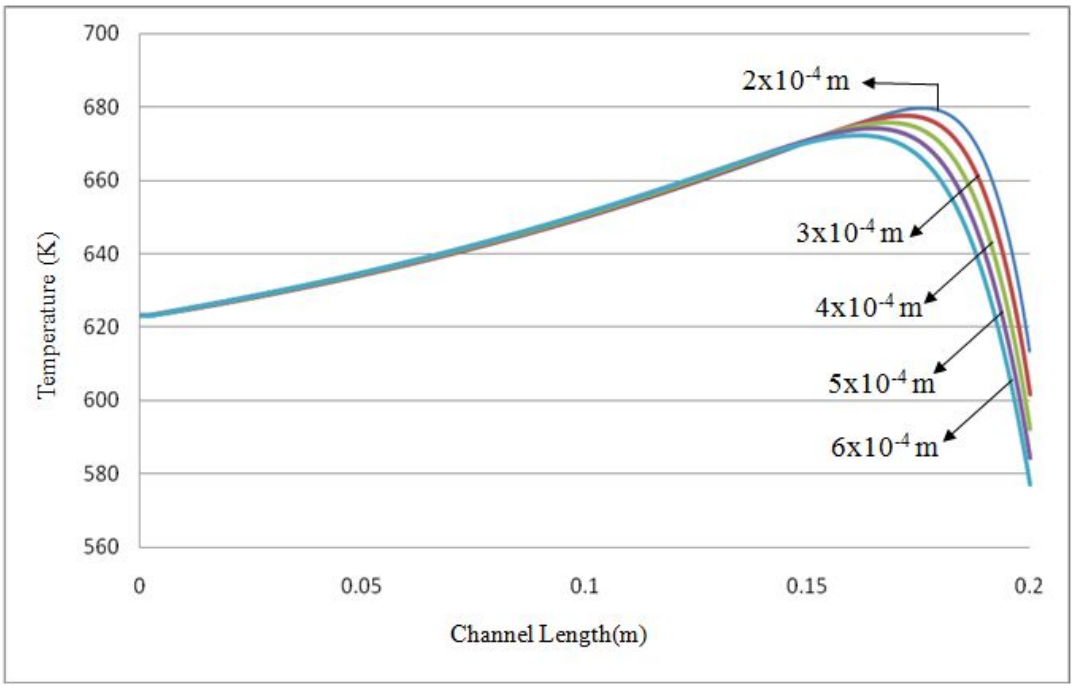

Figure 4.7. Effect of change of reactor wall thickness on temperature profile

Conduction parameter, λ, is used to define the heat transfer relation between fluids and the wall, and to interpret the trends observed in Figure 4.7. In order to discuss the reasons of such profile, thermal properties of the fluids in both channels should be considered as the wall material is kept the same in each simulation. Also, the thermal diffusivity, α, of the fluids should be taken into account. Calculated values of the k, h, λ and α are given in Table 4.1.

Considering the data from Table 4.1, an explanation for Figure 4.1 can be achieved. Conduction parameters related to both channels increase with increasing wall thickness, and indicate higher amounts of heat loss from both channels since conduction parameter is a measure showing how much of available energy can be transferred through

Table 4.1. Calculated properties of fluids at different wall thickness values

Thickness(μm)	200	300	400	500	600
λ_{CO+H_2}	3.08	4.62	6.16	7.70	9.24
λ_{steam}, x10^{-2}	0.45	0.67	0.89	1.11	1.33
k_{CO+H_2}, x10^2 W/(mK)	9.43	9.42	9.41	9.40	9.39
k_{steam}, x10^2 W/(mK)	5.03	5.02	5.00	4.99	4.97
h_{CO+H_2}, W/(m^{2}K) x10^{-2}	3.17	3.17	3.17	3.16	3.16
h_{steam}, W/(m^{2}K) x10^{-1}	7.22	7.23	7.21	7.18	7.16
α_{CO+H_2}, x10^6 m^2/s	8.50	8.48	8.46	8.44	8.42
α_{steam}, x10^5 m^2/s	9.08	9.04	8.98	8.94	8.88

the wall (Peterson, 1999). This change in conduction parameter also means that, as thickness of the wall is decreased, fluids try to preserve their hot/cold characteristic. Since reaction channel in 200 μm case does not dissipate the generated heat as well as it is in 600 μm case, it is logical to expect to reach the highest temperature in former case.

Conduction parameter based on cooling channel involving steam has a higher value than that of the reaction mixture. This shows that cooling channel is more effective in terms of heat transfer, i.e. coolant is more dominant in system to decide on the faith of the reaction temperature profile. This fact can also be observed by comparing thermal diffusivity values of two gas streams. Thermal diffusivity, α, is defined as the ratio of heat conducted through the material to heat stored per unit volume. This means that a larger thermal diffusivity results in faster diffusion of heat into the material due to the high thermal conductivity of the fluid. Smaller α, on the other hand, indicates that a big part of the heat is absorbed by the material and only a small portion is conducted through. (Incropera *et al.*, 2007) Comparable thermal diffusivity values in Table 4.1 show that reaction mixture is more likely to store its heat whereas

steam readily transfers heat to reaction channel.

Table 4.2. Summary of the effect of wall thickness on FT performance

Thickness (μm)	X_{CO} %	rxn T_{ave} (K)	cool T_{ave} (K)	F_{HC} total (mol/s) x10^6	Olefins (mol/s) x10^8	Paraffins (mol/s) x10^6	O/P ratio x10^1
200	5.17	649.72	639.70	1.55	8.64	1.46	0.59
300	5.15	648.88	637.75	1.53	8.65	1.44	0.60
400	5.10	648.05	636.04	1.50	8.66	1.42	0.61
500	5.10	647.22	634.50	1.48	8.67	1.40	0.62
600	5.06	646.31	632.98	1.46	8.69	1.38	0.63

Temperature profiles in Figure 4.7 shows that the exothermal heat release becomes more significant towards the end of the reactor. Looking at Figure 4.7, it is obvious that the length between the exit of the hot channel (or the entrance of the cold channel) the locus of the maximum temperature moves inwards to the left. Additionally, maximum temperature within the channel and the outlet temperature of the hot stream decrease with increasing thickness. This can be explained by the fact that as thickness increases, the amount of heat transfer through the wall increases (Norton and Vlachos, 2003; Norton and Vlachos, 2004; Stutz and Poulikakos, 2005) from both channels, cooling channel being the more effective one. Steam, being more conservative in terms of keeping its coldness as is can be understood from the comparison of k and h values of both gases, gains control more effectively as thickness is increased. As steam preserves its coldness, it suppresses reaction from reaching higher levels of temperature by the fact that its ability to transfer its coldness is more. Consequently the maximum temperature in the channel stays at a lower value, and the average temperature in the channel decreases as thickness increases. In other words, as thickness decreases, the amount of heat transferred to cold side increases and cooling fluid is heated up in a shorter distance. Thus, heated cooling fluid uses this heat to increase the temperature of the reactant fluids through the entrance of the channel, enabling the temperature to reach higher values as reactions move forward as can be seen from the figure.

Table 4.3. Effect of wall thickness on the molar flow of species other than the hydrocarbons

Thickness (μm)	CO (mol/s) x10^4	H_2 (mol/s) x10^4	CO_2 (mol/s) x10^6	H_2O (mol/s) x10^7
200	1.53	3.09	1.24	4.19
300	1.53	3.09	1.22	4.13
400	1.53	3.09	1.20	4.08
500	1.53	3.09	1.18	4.03
600	1.54	3.09	1.17	3.99

Looking at Table 4.1, it can be seen that the thermal conductivity and heat transfer coefficient of the reaction mixture are higher than those of the cooling fluid. Thus, reaction mixture is more eligible to distribute heat in channel better. Additionally, steam will preserve its cold characteristic more, and as thickness is increased, its effect on reaction channel will be higher.

Table 4.4. Effect of wall thickness on the molar flow of olefins

Thickness (μm)	C_2H_4 (mol/s) x10^8	C_3H_6 (mol/s) x10^9	C_4H_8 (mol/s) x10^{10}	C_5H_{10} (mol/s) x10^{11}	C_6H_{12} (mol/s) x10^{11}	C_7H_{14} (mol/s) x10^{11}
200	8.16	4.30	3.96	0.97	4.83	3.06
300	8.15	4.38	4.29	1.14	5.81	3.72
400	8.15	4.46	4.58	1.29	6.68	4.30
500	8.15	4.53	4.86	1.42	7.49	4.84
600	8.15	4.61	5.13	1.55	8.25	5.35

It is also observed that as thickness increases, the average temperatures of the reaction channel and the cooling channel decrease, leading to decreases in CO conversion, which is usually used in literature to define the conversion level of the FT

Table 4.5. Effect of wall thickness on the molar flow of paraffins

Thickness (μm)	CH_4 (mol/s) x10^6	C_2H_6 (mol/s) x10^8	C_3H_8 (mol/s) x10^{10}	C_4H_{10} (mol/s) x10^{11}	C_5H_{12} (mol/s) x10^{11}	C_6H_{14} (mol/s) x10^{11}	C_7H_{16} (mol/s) x10^{11}
200	1.45	1.02	5.89	6.78	2.19	1.24	0.84
300	1.43	1.03	6.06	7.52	2.59	1.50	1.03
400	1.41	1.03	6.22	8.18	2.96	1.73	1.19
500	1.39	1.03	6.37	8.80	3.29	1.94	1.34
600	1.37	1.03	6.52	9.39	3.61	2.14	1.48

synthesis, and in the total amount of hydrocarbons produced (Table 4.2). However, as an expected behavior of the FT process, a shift towards the production of higher hydrocarbons occurs at lower temperatures. Moreover, olefin-to-paraffin ratio increase with decreasing temperature (Table 4.2), as also stated in the literature (Dry, 2004). It can be observed from Table 4.3 that the amounts of produced CO_2 and H_2O also decrease with the decreasing value of average temperature, either.

Additionally, importance of methane for Fischer-Tropsch synthesis can be observed from Table 4.5. The produced amount of methane is almost 100 times higher than the closest produced amount of any other hydrocarbon product. And as average temperature decreases by the increase in wall thickness, the amount of produced CH_4 decreases, however, there are significant increases in amounts of C_{3+} products, either olefins or paraffins, as can be observed from Tables 4.4 and 4.5.

4.2. Effect of reactor wall material

Temperature profiles of the FT channel, obtained with different wall materials, are given in Figure 4.8. It is understood from Figure 4.8 that as thermal conductivity of the material increases the maximum temperature in the reaction channel decreases and temperature profile gains a smoother path. The data required to interpret the trends of the profiles in Figure 4.8 are provided in Table 4.6. Conduction parameters

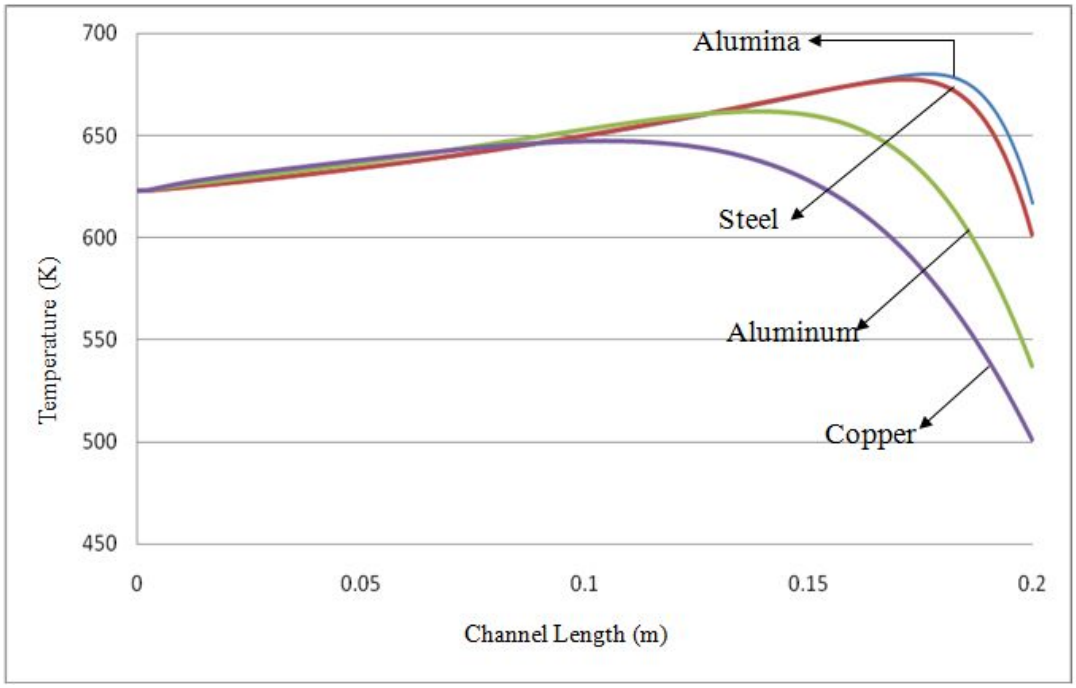

Figure 4.8. Effect of reactor wall material on temperature profile of the FT channel

of both channels increase as conductivity of the wall increases, which indicates that heat loss from both channels is becoming higher. As explained in Section 4.1, this means that fluids preserve their hot/cold characteristic as conductivity of the wall is decreased. As the thermal conductivity of the material increases, its ability to transfer heat increases; when using alumina as the wall material, reaction channel cannot dissipate the generated heat as well as the case when copper is used. This brings out the fact that the maximum and the average temperature of reaction channel will be higher when using materials with low conductivity. (Norton and Vlachos, 2003; Norton and Vlachos, 2004; Stutz and Poulikakos, 2005)

In all simulations, steam always has higher conduction parameter values than reaction mixture, which can be counted as a measure of effectiveness in terms of heat transfer. This fact can also be observed by comparing thermal diffusivity values of two streams.

Table 4.6. Calculated properties of fluids for different wall materials

	alumina	AISI	aluminum	copper
k, W/(mK)	27	44.5	201	400
λ_{CO+H_2} x10^{-1}	0.28	0.46	2.09	4.16
λ_{steam} x10^{-2}	0.24	0.39	1.77	3.53
k_{CO+H_2}, W/(mK) x10^2	9.43	9.42	9.32	9.17
k_{steam}, W/(mK) x10^2	5.04	5.02	4.87	4.70
h_{CO+H_2}, W/(m^2K) x10^{-2}	3.17	3.17	3.15	3.11
h_{steam}, W/(m^2K) x10^{-1}	7.25	7.23	7.08	6.91
α_{CO+H_2}, (m^2/s) x10^6	8.45	8.44	8.36	8.24
α_{steam}, (m^2/s) x10^5	9.00	8.97	8.71	8.42

From the data in Table 4.6, it can be concluded that although the amount of heat flow increases with increasing conductivity, the transportation of the transferred heat within the fluids is deterministic on the faith of the processes. Reaction mixture has higher k and h values, indicating that the heat transported into this mixture is distributed with ease compared to steam. This means that cooling is more dominant than heating(i.e. remains as an effective heat sink), since steam is able to preserve its cold nature. So it is obvious that as thermal conductivity of the wall increases, temperature profile should become smoother and both the maximum and the outlet temperatures of the reaction channel should decrease as it is in Figure 4.8.

Table 4.7. Summary of the effect of wall material on FT performance

Material	X_{CO} %	rxn T_{ave} (K)	cool T_{ave} (K)	F_{HC} total (mol/s) x10^6	Olefins (mol/s) x10^8	Paraffins (mol/s) x10^6	O/P ratio x10^1
Alumina	5.18	649.9	640.19	1.56	8.65	1.47	0.59
AISI	5.15	648.88	637.75	1.53	8.65	1.44	0.60
Aluminum	4.92	638.83	621.52	1.31	8.73	1.23	0.71
Copper	4.63	623.92	602.93	1.0	8.80	0.97	0.91

Similar to the trend noted in Section 4.1, value of the maximum temperature, the distance of the locus of maximum temperature from the entrance of the FT channel and the exit temperature respond similar trends against change in the wall conductivity; values of all of the outcomes decrease with increasing wall conductivity. When using material with high conductivity, reaction mixture is forced to transfer its heat to steam before reactions move forward and release more heat. Hence, temperature within the reaction channel stays at lower values.

Table 4.8. Effect of wall material on the molar flow of species other than the hydrocarbons

Material	CO (mol/s) x10^4	H_2 (mol/s) x10^4	CO_2 (mol/s) x10^6	H_2O (mol/s) x10^7
Alumina	1.53	3.09	1.24	4.20
AISI	1.53	3.09	1.22	4.13
Aluminum	1.54	3.09	1.05	3.71
Copper	1.54	3.10	0.84	3.32

Table 4.7 summarizes the impact of the wall thermal conductivity on FT performance. One important result is that using copper as wall material results in almost isothermal operation as the average temperature in the channel is calculated to be 623.92 K, while the feed temperature is at 623 K. The effect of FT temperature, af-

Table 4.9. Effect of wall material on the molar flow of olefins

Material	C_2H_4 (mol/s) x10^8	C_3H_6 (mol/s) x10^9	C_4H_8 (mol/s) x10^9	C_5H_{10} (mol/s) x10^{10}	C_6H_{12} (mol/s) x10^{10}	C_7H_{14} (mol/s) x10^{10}
Alumina	8.16	4.29	0.39	0.94	0.46	0.29
AISI	8.15	4.38	0.43	1.14	0.5	0.37
Aluminum	8.09	5.20	0.71	2.49	1.36	0.89
Copper	7.95	6.58	1.14	4.27	2.35	1.52

fected by wall thermal conductivity, on hydrocarbon product distribution can clearly be observed; the amounts of produced olefins (alkenes) increase, whereas those of paraffins (alkanes) decrease (Table 4.7).

Table 4.10. Effect of wall material on the molar flow of paraffins

Material	CH_4 (mol/s) x10^6	C_2H_6 (mol/s) x10^8	C_3H_8 (mol/s) x10^9	C_4H_{10} (mol/s) x10^{10}	C_5H_{12} (mol/s) x10^{10}	C_6H_{14} (mol/s) x10^{11}	C_7H_{16} (mol/s) x10^{11}
Alumina	1.46	1.02	0.59	0.67	0.21	1.19	0.80
AISI	1.43	1.03	0.61	0.75	0.26	1.50	1.03
Aluminum	1.21	1.05	0.77	1.38	0.59	3.56	2.47
Copper	0.96	1.08	1.03	2.27	1.01	6.11	4.22

The decrease in the average FT channel temperature at higher wall conductivities results also in lower CO conversion levels, in higher olefin-to-paraffin ratios and a shift from lower carbon numbers to higher in terms of production (Table 4.7)(Dry, 2002; Ji et al., 2001; Schulz, 1999; Van der Laan and Beenackers, 1999b). From Tables 4.9 and 4.10, it can be seen that the productions of CH_4, C_2H_6, C_2H_4 decrease, C_3H_8 and C_3H_6 productions increase slightly, whereas the produced amounts of rest of the hydrocarbons are almost doubled with the decrease in average temperature. Similar to the results in Section 4.1, CO_2 and H_2O production also decrease with the decreasing value of average temperature (Table 4.8).

4.3. Effect of cooling fluid type

Temperature profiles of the FT channel, obtained with different coolants, are given in Figure 4.9. The temperature profiles show that maximum temperature decrease in the order of methane, air and steam. However, the distance between the point where the maximum temperature is reached and the entrance of the FT channel does not follow the same order; distance decreases in the order of steam, methane and air. This order is also valid for the exit temperature (Figure 4.9). Different from the

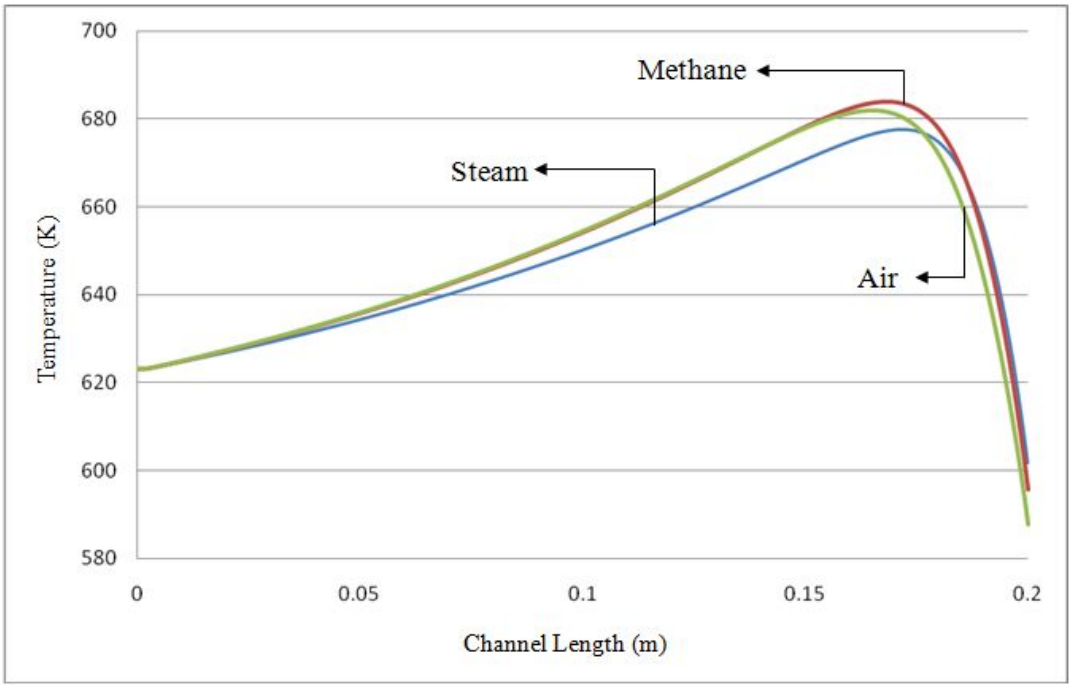

Figure 4.9. Effect of cooling fluid type on temperature profile of the FT channel

previous two cases, there is not a direct explanation of this figure, as there is no distinct property readily available to reach a conclusion about the profiles obtained in Figure 4.9. The calculated properties that can be helpful in understanding the differences between the profiles are given in Tables 4.11 and 4.12.

In Figure 4.9, it is observed that using methane results in the highest temperature peak, but the point where the peak is located in the reactor is in between the peaks of air- and steam-cooled cases. The temperature profiles for air and methane resemble each other, whereas steam has somewhat different profile with a less pro-

Table 4.11. Calculated properties of fluids at inlet conditions

Cooling fluid	steam	air	CH_4
k_{CO+H_2}, W/(mK) x10^2	9.16	9.16	9.16
k, W/(mK) x10^2	2.67	3.02	4.83
h_{CO+H_2}, W/(m^2K) x10^{-2}	3.15	3.15	3.15
h, W/(m^2K) x10^{-1}	5.66	6.15	9.29
$C_{P_{CO+H_2}}$, J/(mol K) x10^{-3}	2.81	2.81	2.81
C_P, J/(mol K) x10^{-3}	1.64	1.02	2.49
ρ, (kg/m^3)	0.57	0.93	0.52
α_{CO+H_2}, (m^2/s) x10^6	7.91	7.91	7.91
α, (m^2/s) x10^5	2.81	3.17	3.77

nounced temperature rise. Looking at the reaction channel outlet, it is seen that the exit temperature falls down as cooling fluid is changed in the following order of steam, methane and air.

Methane with its high heat capacity is a good candidate to be a cooling fluid. Thus, it would be logical to expect the peak in the temperature to shift leftwards as observed in Figure 4.9. However, the maximum temperature in methane is higher than the ones observed for steam and air. This figure can be explained by considering the data in Tables 4.11 and 4.12.

Comparing k and h values of coolants at inlet and average temperatures, it is seen that the decreasing order of methane, air, steam changes to methane, steam and air (Tables 4.11 and 4.12). As methane always has the highest thermal conductivity and heat transfer coefficient at any temperature, it is understood that methane is more efficient in dispersing the heat transferred from hot channel. However, it is seen that,

Table 4.12. Calculated properties of fluids at the average channel temperatures

Cooling fluid	steam	air	CH_4
k_{CO+H_2}, W/(mK) x10^2	9.42	9.44	9.45
k, W/(mK) x10^2	5.02	4.53	9.71
h_{CO+H_2}, W/(m^2K) x10^{-2}	3.17	3.17	3.18
h, W/(m^2K) x10^{-2}	0.72	0.69	1.38
$C_{P_{CO+H_2}}$, J/(mol K) x10^{-3}	2.81	2.81	2.81
C_P, J/(mol K) x10^{-3}	1.64	1.07	3.45
ρ, (kg/m^3)	0.34	0.55	0.30
α_{CO+H_2}, (m^2/s) x10^6	8.44	8.52	8.54
α, (m^2/s) x10^5	8.97	7.77	9.38

reaction channel achieves higher average temperature (Table 4.13)when using methane as ccoolant which is a fact that requires further explanation.

Considering the case of steam and air, it can be said that at lower temperatures, air is able to disperse the transferred heat within itself, but as temperature increases, steam becomes more efficient than air in terms of distributing heat. The change in temperature profile of the case when using steam, starting from the below then taking place between the cases using air and methane(Figure 4.9), can be explained considering this change in h and k values of air and steam, as observed in Tables 4.11 and 4.12.

Density is one of the properties that can be used to compare the heat transfer capabilities of fluids. In such a system, high density indicates the presence of more mass for heat removal (Fan et.al, 2007). Thus, air, having the highest density, is capable of lowering the reaction channel outlet more than steam or methane. Additionally, the increase in temperature of air at the inlet of cooling channel is more gradual than it is

in steam or methane case (Figure 4.9).

When thermal diffusivities of coolants at the inlet and average temperature are compared, it is noted that thermal diffusivity of steam evaluated at the average temperature is more than 3 times higher than the thermal diffusivity evaluated at the inlet temperature. The increases in the cases of air and methane are approximately 2.5 times the values at inlet temperature (Tables 4.11 and 4.12). In the same manner, the increase in thermal diffusivity of reaction mixture stays at a lower value than it is for air or methane. From these results it can be claimed that, compared to air and methane, steam is ready to absorb heat but since it is not eligible to carry too much heat load, it starts to diffuse heat within itself and reaches equilibrium at a lower temperature, and the outlet temperature of reaction channel, being close to average temperature, stays at a higher value than it is in air or methane cases.

Methane and air seem to act like similar in terms of thermal diffusivities. However, air, having a lower thermal diffusivity value, tends to preserve its cold nature more. Although, specific heat capacity of methane is higher, the amount of methane present in terms of mass in the system can never exceed the amounts of steam or air. Thus, having a higher thermal diffusivity, methane easily gets heated up and reaches the maximum temperature.

Table 4.13. Summary of the effect of coolant fluid type on FT performance

Cooling fluid	X_{CO} %	rxn T_{ave} (K)	cool T_{ave} (K)	F_{HC} total (mol/s) x10^6	Olefins (mol/s) x10^8	Paraffins (mol/s) x10^6	O/P ratio x10^1
steam	5.15	648.88	637.75	1.53	8.65	1.44	0.60
air	5.18	650.85	637.62	1.56	8.35	1.47	0.57
CH_4	5.21	651.91	641.54	1.58	8.31	1.50	0.55

Table 4.14. Effect of coolant fluid type on the molar flow of species other than the hydrocarbons

Cooling fluid	CO (mol/s) x10^4	H_2 (mol/s) x10^4	CO_2 (mol/s) x10^6	H_2O (mol/s) x10^7
steam	1.53	3.09	1.22	4.13
air	1.53	3.09	1.24	4.16
CH_4	1.53	3.09	1.26	4.22

Increase in CO conversion level and decrease in olefin to paraffin ratio are observed with increase in average temperature of reaction mixture (Table 4.13) (Dry, 2004). From the molar flow amounts given in Tables 4.15 and 4.16, it can be observed that, high temperature favors methane formation, and similar to the change in temperature profile of the case when using air, as can be seen in Figure 4.9, the produced amounts of olefins and paraffins show a differing pattern. The increase in average temperature of the channel results in an increase in the amount of CO_2 and H_2O produced (Table 4.14).

Table 4.15. Effect of coolant fluid type on the molar flow of olefins

Cooling fluid	C_2H_4 (mol/s) x10^8	C_3H_6 (mol/s) x10^9	C_4H_8 (mol/s) x10^{10}	C_5H_{10} (mol/s) x10^{10}	C_6H_{12} (mol/s) x10^{11}	C_7H_{14} (mol/s) x10^{11}
Steam	8.15	4.38	4.29	1.14	5.81	3.72
Air	7.86	4.21	4.62	1.40	7.41	4.78
CH_4	7.84	4.09	4.24	1.23	6.45	4.18

Table 4.16. Effect of coolant fluid type on the molar flow of paraffins

Cooling fluid	CH_4 (mol/s) x10^6	C_2H_6 (mol/s) x10^8	C_3H_8 (mol/s) x10^{10}	C_4H_{10} (mol/s) x10^{11}	C_5H_{12} (mol/s) x10^{11}	C_6H_{14} (mol/s) x10^{11}	C_7H_{16} (mol/s) x10^{11}
steam	1.43	1.03	6.06	7.52	2.59	1.50	1.03
air	1.46	0.98	5.91	8.45	3.24	1.92	1.32
CH_4	1.49	0.98	5.69	7.65	2.84	1.67	1.16

4.4. Effect of side length of the cooling channel

The results related to the simulations to observe the effect of cooling channel side length on the system are summarized in this subsection. In order to examine the effect of change in cooling channel side length, three different cases are simulated, keeping a different variable - mass flow rate, Reynolds number, linear velocity - constant at each run.

4.4.1. Case I: Effect of side length when mass flow rate is constant

Temperature profiles of the reaction channel, obtained with different cooling channel side lengths while mass flow rate is kept constant, are given in Figure 4.10. It is observed that as side length of the coolant channel is decreased, the maximum temperature reached in the reaction channel increases, but its distance from the entrance of the FT channel and the outlet temperature decrease.

From Table 4.17, it is observed that neither k nor h nor α do differ in any of the cases, in which cooling channel side length is changed, significantly, just as the profiles do not. Thus, the explanation of the profiles in Figure 4.10 should be done by other means.

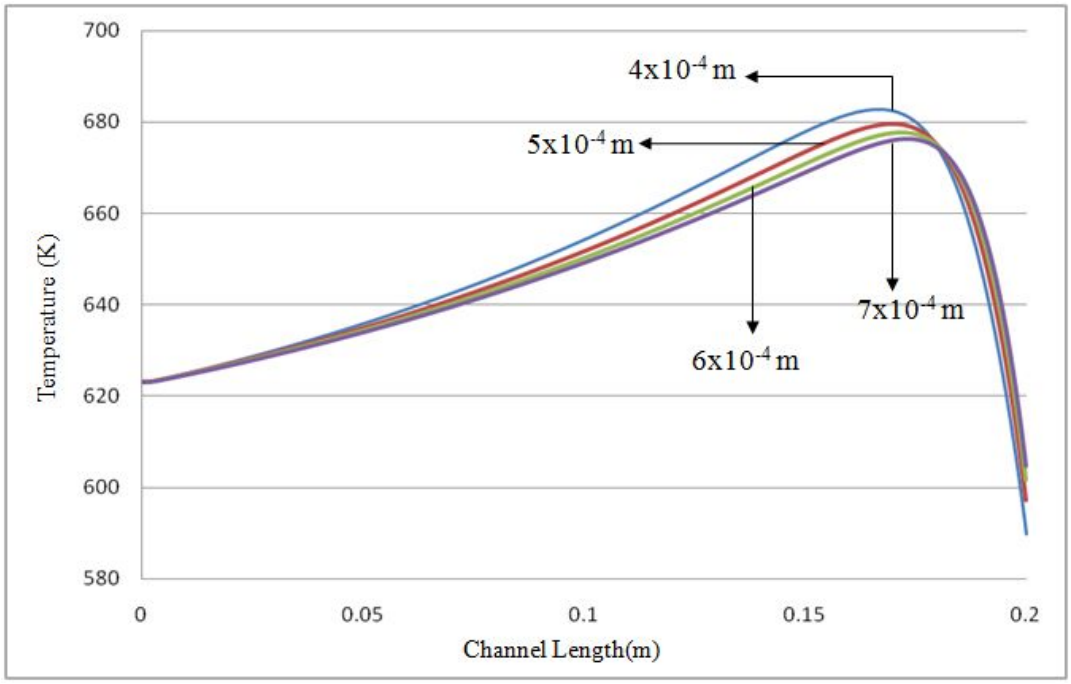

Figure 4.10. Effect of change of cooling channel side length on FT temperature profile when mass flow of coolant is kept constant

It is well known that the linear velocity changes when the diameter is changed but mass flow rate is kept constant; as the diameter is increases, linear velocity decreases and vice versa. Linear velocity is an important parameter for the system as it determines the residence time of the fluid within the channel. At lower side length values, the temperature at the FT channel exit can be expected to be low, since fresh steam enters the channel with a higher velocity.

This observation can be explained by the value of the coolant-side heat transfer coefficient at the entrance zone, which is improved by mixing at high velocities.When linear velocity is high, fresh stream can move inwards from the cooling channel inlet, and the distance of the locus of the maximum temperature from the entrance of the FT channel can decrease.

Table 4.17. Calculated properties of fluids for Case I

Side length (μm)	400	500	600	700
k_{CO+H_2}, W/(mK) x10^2	9.44	9.43	9.42	9.41
k_{steam}, W/(mK) x10^2	5.03	5.02	5.02	5.01
h_{CO+H_2}, W/(m^{2}K) x10^{-2}	3.17	3.17	3.17	3.17
h_{steam}, W/(m^{2}K) x10^{-1}	7.24	7.23	7.23	7.22
α_{CO+H_2}, (m^2/s) x10^6	8.52	8.50	8.48	8.46
α_{steam}, (m^2/s) x10^5	9.07	9.04	9.04	9.01

However, when linear velocity is low, i.e. residence time is high, steam spends more time in channel, and has the opportunity to have more control on reaction temperature. The outlet temperature obtains a higher value as side length is increased, but the maximum and average temperatures within the channel stay at a lower value (Figure 4.10).

Table 4.18. Summary of the effect of Case I on FT performance

Side length (μm)	X_{CO} %	rxn T_{ave} (K)	cool T_{ave} (K)	F_{HC} total (mol/s) x10^6	Olefins (mol/s) x10^8	Paraffins (mol/s) x10^6	O/P ratio x10^1
400	5.19	651.13	638.89	1.56	8.33	1.48	0.56
500	5.16	649.75	638.21	1.54	8.53	1.46	0.59
600	5.15	648.88	637.75	1.53	8.65	1.44	0.60
700	5.14	648.30	637.42	1.52	8.73	1.43	0.61

As mentioned before, it can be observed from Table 4.18 that the average temperatures in reaction channel for different simulations are very close to each other. Related to this fact, the amount of hydrocarbons produced does not differ much, either. There is a slight decrease in temperature within the system as cooling channel side length is increased, and based on the temperature decrease there is a slight decrease in total hydrocarbon molar flow.

Conversion of CO and the amount of hydrocarbons produced are found to decrease as a result of decrease in average temperature within the channel (Table 4.18). It is also observed that, just like in the other cases, olefin-to-paraffin ratio increases with decreasing temperature, as also confirmed by other studies in the literature (Dry, 2004). The reason of the increase in olefin-to-paraffin ratio can also be observed by the molar flow amounts in Tables 4.18, 4.20 and 4.21.

Table 4.19. Effect of Case I on the molar flow of species other than the hydrocarbons

Side length (μm)	CO (mol/s) x10^4	H_2 (mol/s) x10^4	CO_2 (mol/s) x10^6	H_2O (mol/s) x10^7
400	1.53	3.09	1.25	4.18
500	1.53	3.09	1.23	4.15
600	1.53	3.09	1.22	4.13
700	1.53	3.09	1.21	4.12

The total increase in C_2H_4 and C_3H_6 is more than the total decrease in molar flows of rest of the olefins (Table 4.20) leading to an increase in the total amount of olefins produced by the increase in side length (Table 4.18). However, the increase in side length of the cooling channel, thus the decrease in average FT channel temperature only increases the amounts of produced C_2H_6 and C_3H_8 slightly (Table 4.21). Hence, the total amount of paraffins formed decreases by the increase in side length of the cooling channel (Table 4.18). The amounts of produced CO_2 and H_2O decrease with the decrease in average temperature within reaction channel as side length of cooling

channel is increased (Table 4.19).

Table 4.20. Effect of Case I on the molar flow of olefins

Side length (μm)	C_2H_4 (mol/s) x10^8	C_3H_6 (mol/s) x10^9	C_4H_8 (mol/s) x10^{10}	C_5H_{10} (mol/s) x10^{10}	C_6H_{12} (mol/s) x10^{11}	C_7H_{14} (mol/s) x10^{11}
400	7.85	4.17	4.52	1.36	7.21	4.67
500	8.04	4.30	4.38	1.22	6.34	4.07
600	8.15	4.38	4.29	1.14	5.81	3.72
700	8.23	4.44	4.22	1.08	5.46	3.49

Table 4.21. Effect of Case I on the molar flow of paraffins

Side length (μm)	CH_4 (mol/s) x10^6	C_2H_6 (mol/s) x10^8	C_3H_8 (mol/s) x10^{10}	C_4H_{10} (mol/s) x10^{11}	C_5H_{12} (mol/s) x10^{11}	C_6H_{14} (mol/s) x10^{11}	C_7H_{16} (mol/s) x10^{11}
400	1.47	0.98	5.85	8.26	3.15	1.87	1.29
500	1.45	1.01	5.98	7.80	2.81	1.64	1.12
600	1.43	1.03	6.06	7.52	2.59	1.50	1.03
700	1.42	1.04	6.11	7.33	2.45	1.41	0.96

4.4.2. Case II: Effect of side length when Reynolds number is constant

Temperature profiles of the reaction channel, obtained with different cooling channel side length while Reynolds number is kept constant, are given in Figure 4.11. It is observed that the profiles are almost the same for all cooling channel side lengths. In all simulations, thermal conductivities and heat transfer coefficients are found to be nearly equal for both channels (Table 4.22).

Thermal diffusivity of reaction mixture does not change. Change in thermal diffusivity of coolant is more significant. Thus, as channel side length is increased, steam is able to preserve its cold nature slightly more.

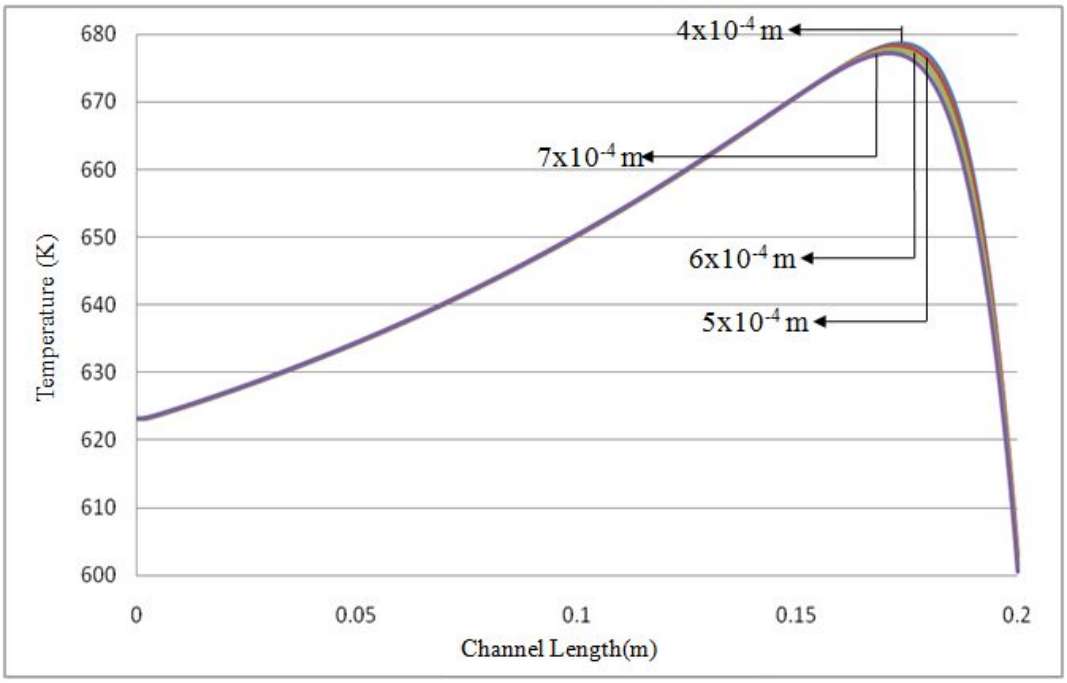

Figure 4.11. Effect of cooling channel side length on FT temperature profiles when Reynolds number is kept constant

When Reynolds number is kept constant, the linear velocity of the coolant changes upon a change in side length of the channel. However, the change between linear velocities related to side length change is not as significant as in the previous case. As explained in Case 1, increase in residence time results in a better control over temperature, but, in this case, as thermal diffusivity of steam gets lower by increase in channel side length, a more effective cooling of the reaction channel is noted. Thus, the maximum and average temperatures within the channel do decrease by increasing channel side length, but without too much difference between the simulations for any side length (Figure 4.11).

It is possible to observe the decreasing pattern in CO conversion level and average temperature in this simulation as well. Since the change in temperatures between different side length trials is not significant, the degree of decrease in CO conversion levels or increase in olefin-to-paraffin ratios is not significant (Table 4.23). As a result of the slight decrease in average temperature within the reaction channel, there is a slight decrease in molar flows of CO_2 and H_2O (Table 4.24). The molar flow of only CH_4

Table 4.22. Calculated properties of fluids for CaseII

Side length (μm)	400	500	600	700
k_{CO+H_2}, W/(mK) x10^2	9.42	9.42	9.42	9.42
k_{steam}, W/(mK) x10^2	5.04	5.03	5.02	5.00
h_{CO+H_2}, W/(m^2K) x10^{-2}	3.17	3.17	3.17	3.17
h_{steam}, W/(m^2K) x10^{-1}	7.25	7.24	7.23	7.21
α_{CO+H_2}, (m^2/s) x10^6	8.48	8.48	8.48	8.48
α_{steam}, (m^2/s) x10^5	9.11	9.08	9.04	8.98

decreases by a negligible amount whereas the molar flows of other products (olefins and paraffins) increase slightly. The amount of increase obtains higher value as carbon number of the product is increased as can be observed in Tables 4.25 and 4.26.

Table 4.23. Summary of the effect of Case II on FT performance

Side length (μm)	X_{CO} %	rxn T_{ave} (K)	cool T_{ave} (K)	F_{HC} total (mol/s) x10^6	Olefins (mol/s) x10^8	Paraffins (mol/s) x10^6	O/P ratio x10^1
400	5.16	649.28	640.51	1.54	8.62	1.45	0.59
500	5.15	649.09	639.16	1.53	8.63	1.44	0.60
600	5.15	648.88	637.75	1.53	8.65	1.44	0.60
700	5.14	648.68	636.31	1.52	8.67	1.43	0.60

Table 4.24. Effect of Case II on the molar flow of species other than the hydrocarbons

Side length (μm)	CO (mol/s) x10^4	H_2 (mol/s) x10^4	CO_2 (mol/s) x10^6	H_2O (mol/s) x10^7
400	1.53	3.09	1.23	4.16
500	1.53	3.09	1.22	4.15
600	1.53	3.09	1.22	4.13
700	1.53	3.09	1.21	4.12

Table 4.25. Effect of Case II on the molar flow of olefins

Side length (μm)	C_2H_4 (mol/s) x10^8	C_3H_6 (mol/s) x10^9	C_4H_8 (mol/s) x10^{10}	C_5H_{10} (mol/s) x10^{10}	C_6H_{12} (mol/s) x10^{11}	C_7H_{14} (mol/s) x10^{11}
400	8.12	4.31	4.12	1.08	5.56	3.59
500	8.14	4.35	4.21	1.11	5.70	3.66
600	8.15	4.38	4.29	1.14	5.81	3.72
700	8.16	4.42	4.36	1.16	5.92	3.78

Table 4.26. Effect of Case II on the molar flow of paraffins

Side length (μm)	CH_4 (mol/s) x10^6	C_2H_6 (mol/s) x10^8	C_3H_8 (mol/s) x10^{10}	C_4H_{10} (mol/s) x10^{11}	C_5H_{12} (mol/s) x10^{11}	C_6H_{14} (mol/s) x10^{11}	C_7H_{16} (mol/s) x10^{11}
400	1.44	1.02	5.94	7.21	2.48	1.44	1.00
500	1.43	1.02	6.00	7.37	2.54	1.47	1.01
600	1.43	1.03	6.06	7.52	2.59	1.50	1.03
700	1.42	1.03	6.12	7.66	2.65	1.52	1.04

4.4.3. Case III: Effect of side length when linear velocity is constant

Temperature profiles of the FT channel, obtained with different cooling channel side lengths while velocity is kept constant, are given in Figure 4.12.

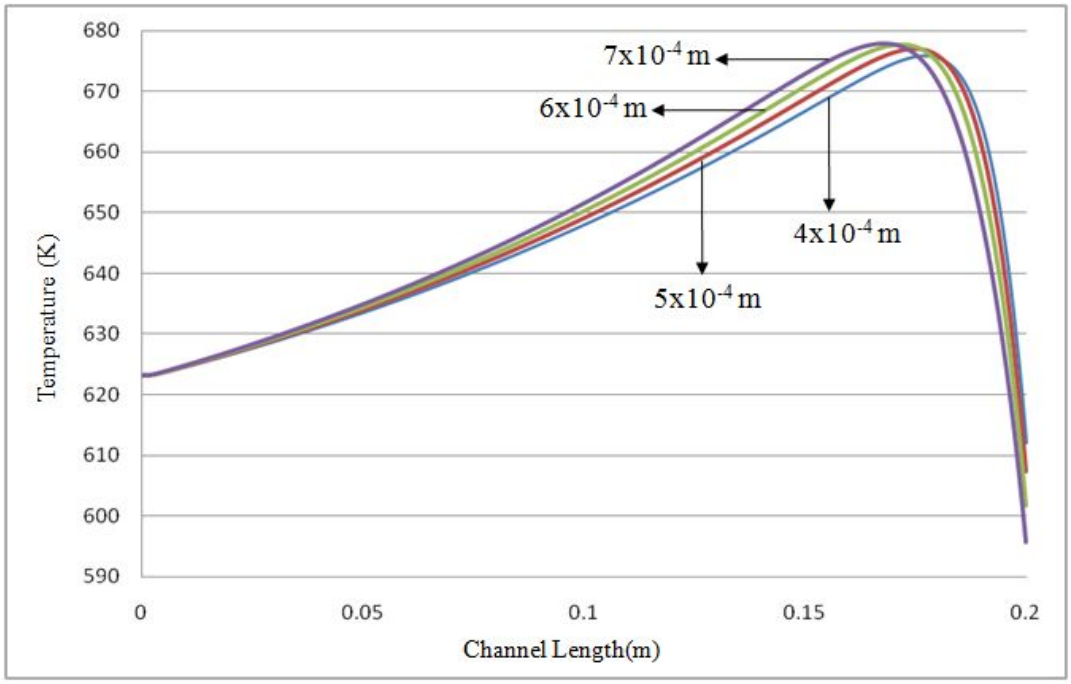

Figure 4.12. Effect of change of cooling channel side length on FT temperature profiles when linear velocity is kept constant

The change in cooling channel side length results in a change in mass flow rate, since linear velocity is constant. Mass flow increases with increased side length of cooling channel and vice versa. Increased mass flow enables better heat removal and control of temperature, since there is more coolant in the channel. Thus, the outlet temperature of reaction channel decreases as the cooling channel side length is increased. Heat exchange between channels becomes gradual as side length is increased, but as thermal diffusivity of both streams tends to decrease slightly (Table 4.27), it should be expected that the maximum temperature should increase slightly, just as it is observed in Figure 4.12.

As observed in previous cases, increase in temperature results in an increase in CO conversion and a decrease in olefin-to-paraffin ratio. Since the change in temperature

Table 4.27. Calculated properties of fluids for Case III

Side length (μm)	400	500	600	700
k_{CO+H_2}, W/(mK) x10^2	9.41	9.41	9.42	9.42
k_{steam}, W/(mK) x10^2	5.05	5.04	5.02	4.99
h_{CO+H_2}, W/(m^2K) x10^{-2}	3.16	3.16	3.17	3.17
h_{steam}, W/(m^2K) x10^{-1}	7.24	7.23	7.21	7.19
α_{CO+H_2}, (m^2/s) x10^6	8.50	8.48	8.48	8.47
α_{steam}, (m^2/s) x10^5	9.11	9.08	9.04	8.98

in runs with different side lengths is not so significant, the change in temperature or olefin to paraffin ratio is also small (Table 4.28). Similarly, the decrease in produced amounts of CO_2 and H_2O is almost negligible by the increase in side length (Table 4.29).

Table 4.28. Summary of the effect of Case III on FT performance

Side length (μm)	X_{CO} %	rxn T_{ave} (K)	cool T_{ave} (K)	F_{HC} total (mol/s) x10^6	Olefins (mol/s) x10^8	Paraffins (mol/s) x10^6	O/P ratio x10^1
400	5.14	647.96	641.41	1.52	8.79	1.43	0.62
500	5.14	648.50	639.88	1.52	8.72	1.44	0.61
600	5.15	648.88	637.75	1.53	8.65	1.44	0.60
700	5.15	649.04	635.00	1.52	8.61	1.44	0.60

As expected, the temperature rise leads to an increase in produced methane and C_2 hydrocarbons but to a decrease in C_{3+} hydrocarbons (Tables 4.30 and 4.31). However, the increase and decrease are in small amounts due to the small change in temperature profiles.

Table 4.29. Effect of Case III on the molar flow of species other than the hydrocarbons

Side length (μm)	CO (mol/s) x10^4	H_2 (mol/s) x10^4	CO_2 (mol/s) x10^6	H_2O (mol/s) x10^7
400	1.53	3.09	1.21	4.14
500	1.53	3.09	1.21	4.14
600	1.53	3.09	1.22	4.13
700	1.53	3.09	1.22	4.11

Table 4.30. Effect of Case III on the molar flow of olefins

Side length (μm)	C_2H_4 (mol/s) x10^8	C_3H_6 (mol/s) x10^9	C_4H_8 (mol/s) x10^{10}	C_5H_{10} (mol/s) x10^{10}	C_6H_{12} (mol/s) x10^{11}	C_7H_{14} (mol/s) x10^{11}
400	8.29	4.43	3.96	0.95	4.72	3.04
500	8.22	4.39	4.09	1.03	5.22	3.36
600	8.15	4.38	4.29	1.14	5.81	3.72
700	8.10	4.40	4.54	1.26	6.48	4.13

Table 4.31. Effect of Case III on the molar flow of paraffins

Side length (μm)	CH_4 (mol/s) x10^6	C_2H_6 (mol/s) x10^8	C_3H_8 (mol/s) x10^{10}	C_4H_{10} (mol/s) x10^{11}	C_5H_{12} (mol/s) x10^{11}	C_6H_{14} (mol/s) x10^{11}	C_7H_{16} (mol/s) x10^{11}
400	1.42	1.05	6.05	6.72	2.14	1.22	0.85
500	1.43	1.03	6.03	7.07	2.35	1.35	0.93
600	1.43	1.03	6.06	7.52	2.59	1.50	1.03
700	1.43	1.02	6.14	8.08	2.88	1.66	1.13

4.5. Effect of coolant mass flow rate

Results of the simulations presenting the effect of coolant mass flow rate on the system are summarized in this subsection. Mass flow rates are changed via increasing the linear velocity of the coolant keeping the side length of cooling channel as constant. Temperature profiles of the reaction channel, obtained with different linear velocities, are given in Figure 4.13.

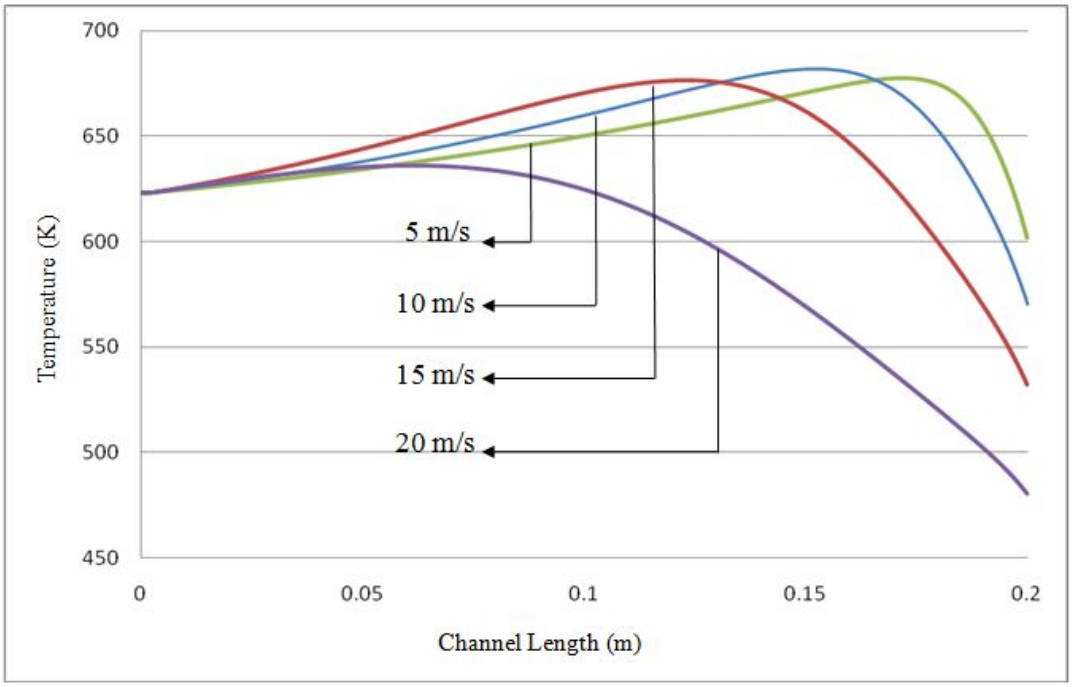

Figure 4.13. Effect of change of coolant mass flow rate on temperature profile

Temperature profiles show that increasing linear velocity results in a decrease in outlet and maximum temperatures. Also, the distance of maximum temperature point from entrance of the reaction channel inlet decreases with increasing mass flow rate.

The increase in the amount of flow enables steam to absorb more heat from reaction channel. Additionally, thermal diffusivity values of steam in each run shows that steam is more likely to preserve its colder nature more as linear velocity is increased (Table 4.32). Thus, temperature of the FT channel cannot reach higher values, avoiding the reactions to proceed (Figure 4.13). Decrease in the FT temperature results in lower CO conversions and higher olefin-to-paraffin ratios, as expected (Table 4.33).

Table 4.32. Effect of coolant mass flow rate on FT temperature profiles

Linear velocity (m/s)	5	10	15	20
k_{CO+H_2}, W/(mK) x10^2	9.42	9.43	9.36	8.91
k_{steam}, W/(mK) x10^2	5.02	5.04	4.78	4.26
h_{CO+H_2}, W/(m^2K) x10^{-2}	3.17	3.17	3.16	3.13
h_{steam}, W/(m^2K) x10^{-1}	7.21	9.15	1.02	1.07
α_{CO+H_2}, (m^2/s) x10^6	8.48	8.50	8.35	7.43
α_{steam}, (m^2/s) x10^5	9.04	8.96	8.26	6.70

Considering that the feed temperature is 623 K, isothermal operation for reaction channel may be achieved by choosing a linear velocity between 15 and 20 m/s.

Table 4.33. Linear velocity change summary

Linear velocity (m/s)	X_{CO} %	rxn T_{ave} (K)	cool T_{ave} (K)	F_{HC} total (mol/s) x10^6	Olefins (mol/s) x10^8	Paraffins (mol/s) x10^6	O/P ratio x10^1
5	5.15	648.88	637.75	1.53	8.65	1.44	0.60
10	5.16	650.30	629.72	1.54	8.21	1.46	0.56
15	5.02	642.91	611.74	1.41	7.93	1.33	0.60
20	4.22	597.92	553.91	0.70	7.98	0.62	1.30

It can be observed from Table 4.34 that the decrease in average FT channel temperature results in a decrease in CO_2 and H_2O production. Total molar flow of hydrocarbon products decreases with increasing linear velocity as a result of decrease in average temperature within the channel. However, molar flow of hydrocarbons, starting from C_3, increase with an increasing degree of production (Tables 4.35 and 4.36) (Dry, 2002; Ji et al., 2001; Schulz, 1999; Van der Laan and Beenackers, 1999b).

Table 4.34. Change in molar flow of species other than hydrocarbons with coolant linear velocity

Linear velocity (m/s)	CO (mol/s) x10^4	H_2 (mol/s) x10^4	CO_2 (mol/s) x10^6	H_2O (mol/s) x10^7
5	1.53	3.09	1.22	4.13
10	1.53	3.09	1.23	4.06
15	1.54	3.09	1.13	3.76
20	1.55	3.11	0.54	2.77

Table 4.35. Change in molar flow of olefins with linear velocity

Linear velocity (m/s)	C_2H_4 (mol/s) x10^8	C_3H_6 (mol/s) x10^9	C_4H_8 (mol/s) x10^9	C_5H_{10} (mol/s) x10^{10}	C_6H_{12} (mol/s) x10^{10}	C_7H_{14} (mol/s) x10^{10}
5	8.15	4.38	0.43	1.14	0.58	0.37
10	7.68	4.35	0.58	1.97	1.06	0.67
15	7.28	4.87	0.92	3.85	2.18	1.42
20	6.75	8.47	2.08E	9.10	5.29	3.54

Table 4.36. Change in molar flow of paraffins with linear velocity

Linear velocity (m/s)	CH_4 (mol/s) x10^6	C_2H_6 (mol/s) x10^8	C_3H_8 (mol/s) x10^9	C_4H_{10} (mol/s) x10^{10}	C_5H_{12} (mol/s) x10^{10}	C_6H_{14} (mol/s) x10^{10}	C_7H_{16} (mol/s) x10^{10}
5	1.43	1.03	0.61	0.75	0.26	0.15	0.10
10	1.45	0.96	0.63	1.10	0.46	0.27	0.18
15	1.32	0.93	0.77	1.91	0.92	0.56	0.39
20	0.60	1.00	1.47	4.44	2.23	1.41	1.00

4.6. Effect of inlet H_2/CO ratio

Results of simulations presenting the effect of molar inlet H_2/CO ratio on the system are summarized in this subsection. Temperature profiles of the reaction channel, obtained with different linear velocities, are given in Figure 4.14. It can be observed that the outlet and maximum temperatures decrease when increasing H_2/CO ratio of feed.

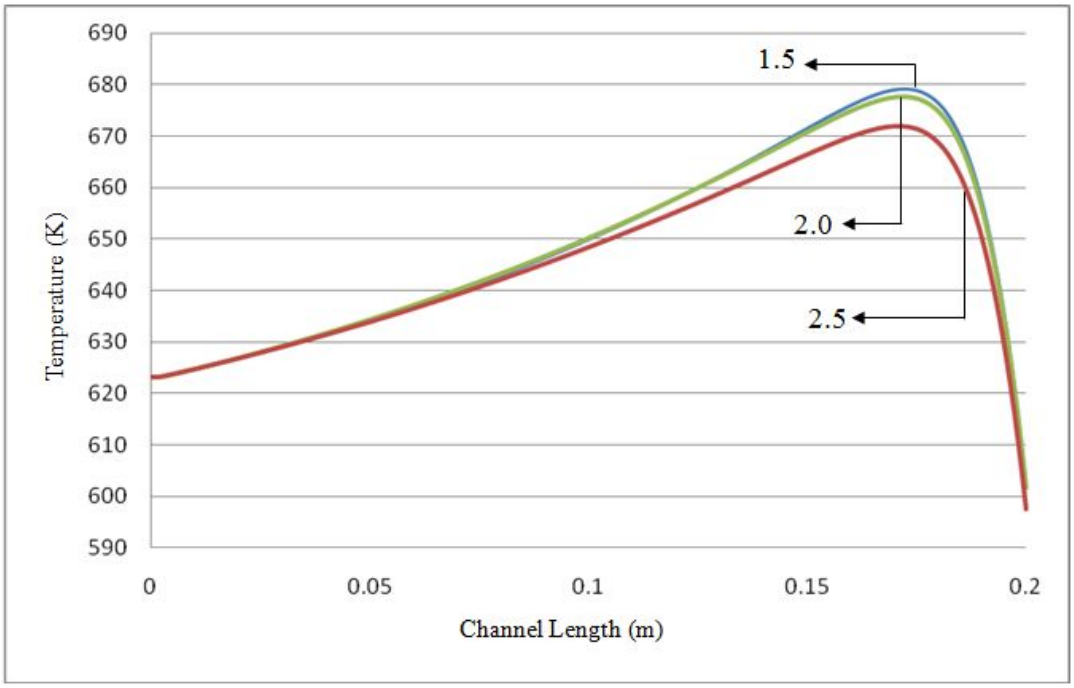

Figure 4.14. Effect of inlet H_2/CO ratio on FT temperature profiles

Conversion of CO is increasing as H_2/CO ratio is increased (Table 4.38) in accordance with the results in literature (Lu and Lee, 2007). Moreover, increase in H_2/CO ratio is claimed to result in a decrease in amount of olefins produced but an increase in the amount paraffins produced (Donnelly and Satterfield, 1993; Dry, 2002). If expressed in other terms, it causes a decrease in olefin to paraffin ratio, just as the simulation results show (Table 4.38).

It can be argued that the olefin-to-paraffin ratio is also affected by the decrease in temperature hence the results may be misleading. However, considering the results obtained upto this point, it can be claimed that olefin to paraffin ratio does not

Table 4.37. Calculated properties of fluids for different H_2/CO ratios

H_2/CO ratio	1.5	2.0	2.5
k_{CO+H_2}, W/(mK) x10^2	9.42	9.42	9.39
k_{steam}, W/(mK) x10^2	5.02	5.02	4.99
h_{CO+H_2}, W/(m^2K) x10^{-2}	3.17	3.17	3.17
h_{steam}, W/(m^2K) x10^{-1}	7.21	7.23	7.28
α_{CO+H_2}, (m^2/s) x10^6	8.45	8.48	8.35
α_{steam}, (m^2/s) x10^5	9.04	9.04	8.62

change significantly with minor changes in average temperature whereas for this case the change can be termed as significant considering the difference between average temperatures. This means that there are other factors affecting the olefin-to-paraffin ratio. Additionally, the difference in the produced olefin amounts between any two run in this simulation is more than that of any other two runs obtained in a simulation, which have more gap between average temperature values. Furthermore, it is a fact that temperature increase results in an increase in CO conversion level, but for this case CO conversion decreases with increasing temperature.

Table 4.38. Summary of the effect of H_2/CO ratio on FT performance

H_2/CO ratio	X_{CO} %	rxn T_{ave} (K)	cool T_{ave} (K)	F_{HC} total (mol/s) x10^6	Olefins (mol/s) x10^7	Paraffins (mol/s) x10^6	O/P ratio x10^1
1.5	4.97	649.14	638.1	1.55	1.13	1.44	0.78
2.0	5.15	648.88	637.75	1.53	0.87	1.44	0.60
2.5	5.21	646.4	634.95	1.38	0.68	1.32	0.52

The conversion of CO is increasing with increased H_2/CO ratio, but total number of hydrocarbons produced decreases. It is mentioned before that the temperature within the reaction channel increases as a result of exothermic reaction occurring. As number of moles of produced hydrocarbons decrease, the heat released via reactions decrease, hence, temperature within reaction channel stays at lower values. This is the reason that average temperature is decreasing by increasing H_2/CO ratio (Table 4.38). As H_2/CO ratio is increased, the amounts of produced CO_2 and H_2O increase as well (Table 4.39). Since the amount of CO present in feed flow is decreasing with the increase in H_2/CO ratio, although the CO conversion seems higher, the amounts of olefins and paraffins are observed to decrease individually in Tables 4.40 and 4.41.

Table 4.39. Effect of H_2/CO ratio on the molar flow of species other than the hydrocarbons

H_2/CO ratio	CO (mol/s) x10^4	H_2 (mol/s) x10^4	CO_2 (mol/s) x10^6	H_2O (mol/s) x10^7
1.5	1.82	2.75	1.34	3.48
2.0	1.53	3.09	1.22	4.13
2.5	1.30	3.27	1.03	4.40

Table 4.40. Effect of H_2/CO ratio on the molar flow of olefins

H_2/CO ratio	C_2H_4 (mol/s) x10^7	C_3H_6 (mol/s) x10^9	C_4H_8 (mol/s) x10^{10}	C_5H_{10} (mol/s) x10^{10}	C_6H_{12} (mol/s) x10^{11}	C_7H_{14} (mol/s) x10^{11}
1.5	1.05	6.42	6.36	1.49	7.10	4.48
2.0	0.82	4.38	4.29	1.14	5.81	3.72
2.5	0.65	3.18	3.15	0.93	4.91	3.16

Table 4.41. Effect of H_2/CO ratio on the molar flow of paraffins

H_2/CO ratio	CH_4 (mol/s) x10^6	C_2H_6 (mol/s) x10^8	C_3H_8 (mol/s) x10^{10}	C_4H_{10} (mol/s) x10^{11}	C_5H_{12} (mol/s) x10^{11}	C_6H_{14} (mol/s) x10^{11}	C_7H_{16} (mol/s) x10^{11}
1.5	1.43	1.17	7.76	9.30	2.83	1.56	1.06
2.0	1.43	1.03	6.06	7.52	2.59	1.50	1.03
2.5	1.31	0.87	4.77	6.23	2.35	1.39	0.96

4.7. Effect of channel wall texture

The results presenting the effect of channel wall texture on the system are summarized in this section. Temperature profiles of the reaction channel, obtained with different channel wall textures, are given in Figure 4.15.

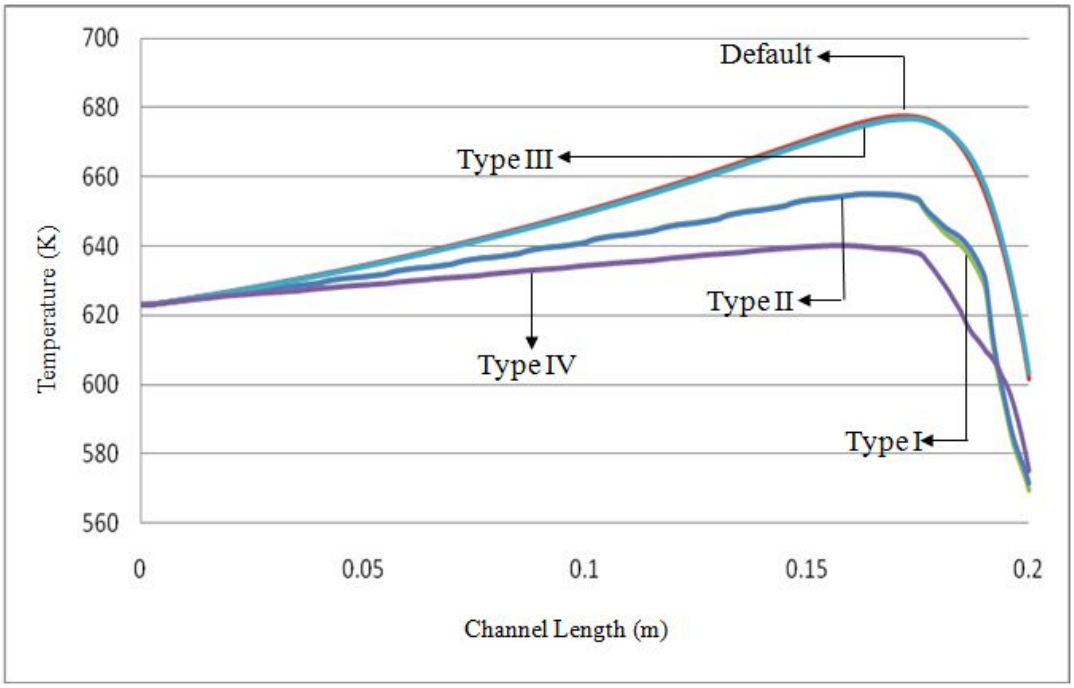

Figure 4.15. Effect of channel wall texture on FT temperature profiles

The effect of using micro-baffles in cooling channel are investigated via comparing default case with Type III and comparing Type I with Type II (Section 3.2.7). The effect of using micro-baffles in reaction channel is investigated via comparing default case with Type I and Type IV.

From Figure 4.15, it can be understood that there is not so much difference between the default case, i.e. no micro-baffles in channels, and using micro-baffles only in cooling channel (Type III); temperature profiles obtained for both runs are almost the same. Similarly, the profile for the run in which micro-baffles are used in reaction channel only (Type I) and the profile in which micro-baffles are used in both channels (Type II) do not differ from each other. Considering these facts, it can be inferred that using micro-baffles in cooling channel do not affect the system.

When micro-baffles are used in reaction channel, the average temperature within channel stays at a lower value than default case (Table 4.42). The case involving thicker micro-baffles (Type IV) leads to lower temperature than the case involving thinner micro-baffles.

Micro-baffles provide higher surface area for heat exchange, thus with same amount of coolant flow it is possible to reach lower temperatures. Moreover the tortuous nature induces static mixing between the baffles and improve heat transfer coefficient. This effect becomes more notable when thicker micro-baffles are used as they enable flow of higher amounts of heat and lower average temperature is reached.

Table 4.42. Summary of the effect of channel property on FT performance

Texture	X_{CO} %	rxn T_{ave} (K)	cool T_{ave} (K)	F_{HC} total (mol/s) x10^6	Olefins (mol/s) x10^8	Paraffins (mol/s) x10^6	O/P ratio x10^1
Default	5.15	648.88	637.75	1.53	8.65	1.44	0.60
Type I	4.33	637.28	625	0.83	6.22	0.77	0.81
Type II	4.34	637.43	627.48	0.83	6.23	0.77	0.81
Type III	5.96	648.58	640.64	1.51	8.63	1.43	0.60
Type IV	26.06	630.49	617.79	0.23	2.11	0.21	1.01

Decrease in average temperature leads to decrease in CO conversions but increase in olefin-to-paraffin ratio (Dry, 2204). As conversion decreases, naturally, the amount

of hydrocarbons produced decreases. However, as can be observed from Tables 4.44 and 4.45 amount of higher hydrocarbons increase, being more in olefins (Dry, 2002; Ji et al., 2001; Schulz, 1999; Van der Laan and Beenackers, 1999b). The decrease in average temperature within FT channel leads to a decrease in the amounts of produced CO_2 and H_2O as can be observed in Table 4.43.

Table 4.43. Effect of channel texture on the molar flow of species other than the hydrocarbons

Texture	CO (mol/s) x10^4	H_2 (mol/s) x10^4	CO_2 (mol/s) x10^6	H_2O (mol/s) x10^7
Default	1.53	3.09	1.22	4.13
Type I	1.55	3.10	0.60	3.11
Type II	1.55	3.10	0.60	3.12
Type III	1.52	3.06	1.21	4.10
Type IV	1.20	2.39	0.12	1.32

Table 4.44. Effect of channel texture on the molar flow of olefins

Texture	C_2H_4 (mol/s) x10^8	C_3H_6 (mol/s) x10^9	C_4H_8 (mol/s) x10^{10}	C_5H_{10} (mol/s) x10^{10}	C_6H_{12} (mol/s) x10^{11}	C_7H_{14} (mol/s) x10^{11}
Default	8.15	4.38	4.29	1.14	5.81	3.72
Type I	5.80	3.77	3.37	0.56	2.01	1.23
Type II	5.81	3.73	3.22	0.53	2.03	1.34
Type III	8.13	4.37	4.24	1.12	5.69	3.62
Type IV	1.90	1.57	2.86	1.10	5.92	3.71

Table 4.45. Effect of channel texture on the molar flow of paraffins

Texture	CH_4 (mol/s) x10^6	C_2H_6 (mol/s) x10^8	C_3H_8 (mol/s) x10^{10}	C_4H_{10} (mol/s) x10^{11}	C_5H_{12} (mol/s) x10^{11}	C_6H_{14} (mol/s) x10^{11}	C_7H_{16} (mol/s) x10^{11}
Default	1.43	1.03	6.06	7.52	2.59	1.50	1.03
Type I	0.76	0.77	5.25	5.35	1.17	0.57	0.41
Type II	0.76	0.77	5.16	5.08	1.13	0.59	0.45
Type III	1.42	1.02	6.03	7.41	2.54	1.46	1.00
Type IV	0.21	0.23	2.17	4.92	2.19E	1.28	0.86

5. CONCLUSIONS AND RECOMMENDATIONS

5.1. Conclusions

The objectives of this study are to understand the effects of operational conditions and microchannel reactor geometry on Fischer-Tropsch synthesis through a parametric study and to gain insight about the possibility of controlling the temperature of the FT reactions. The conclusions drawn from this study can be listed as follows:

- Increasing the thickness of the wall separating the channels results in a decrease in the average temperature within reaction channel. Thus, choosing thicker walls favors isothermal operation.

- The thermal conductivity of the wall is more effective on reaction channel temperature. Choosing higher thermal conductivity values may lead to decrease in temperatures within the channel, even below feed temperature. Material of the wall should be chosen from high conductivity materials with great care not to decrease the temperature too much. Within simulations, copper provided almost an isothermal operation.

- Steam proved to be the most efficient coolant in keeping the average temperature within reaction channel at a closer value to the inlet temperature. Hence, it is a valid choice to define steam as the default coolant in all simulations.

- Changing the cooling channel side length has the least significant effect on system.

- The mass flow rate of the coolant has the most significant effect on the system. As mass flow rate is increased, the average temperature in reaction channel falls even below feed temperature. Thus, mass flow rate of the coolant should be adjusted carefully.

- Any change in H_2/CO ratio means change in feed properties, hence, directly influences the behavior of the reactions involved in Fischer-Tropsch synthesis. As this ratio is increased the average temperature within the reaction channel decreases as a result of decrease in heat released.

- Change in the wall texture affects the temperature of the FT reaction. It is concluded that designing micro-baffles in cooling channel has no effect on the system, whereas existence of micro-baffles in reaction channel as well as their geometry affect the average channel temperature. Using baffles in reaction channel results in decrease in average temperature, and using thicker baffles lowers the average temperature further.

- In all simulations except H_2/CO ratio change, decrease in average temperature results in a decrease in CO conversion level, but an increase in olefin-to-paraffin ratio. Temperature decrease results in a decrase in amount of CH_4 and C_2H_4 produced but an increase in amount of other hydrocarbons.

- Olefin-to-paraffin ratio decreases as H_2/CO ratio is increased, whereas CO conversion increases. With the increase in the ratio, amount of hydrocarbons and CO_2 produced decreases however, amount of produced H_2O increases.

5.2. Recommendations

The recommendations on a possible future work related to this study can be summarized as follows:

- Co-current and cross-current flow modes for the fluids in cooling and FT channels can be applied.

- System can be simulated for hydrocarbons with higher carbon number.

- FT synthesis may be operated at a lower temperature, indicated as low temper-

ature Fischer-Tropsch synthesis.

- Different kinetic expression data and catalyst combinations may be employed to check whether the results are similar to the ones obtained in this study.

APPENDIX A: THERMOPHYSICAL PROPERTIES OF THE SPECIES

Table A.1. Enthalpy of formation of species (Sinnot, 2003)

Species	Δ H (kJ/mol)
CO	-110.62
H_2	-
CO_2	-393.77
H_2O	-242.00
CH_4	-74.86
C_2H_6	-84.74
C_3H_8	-103.92
C_4H_{10}	-126.23
C_5H_{12}	-146.54
C_6H_{14}	-167.30
C_7H_{16}	-187.90
C_2H_4	52.33
C_3H_6	20.43
C_4H_8	-0.13
C_5H_{10}	-20.93
C_6H_{12}	-41.70
C_7H_{14}	-62.34

$$C_p = R(\gamma + \delta T + \xi T^2 + \varphi T^{-2}) \tag{A.1}$$

Table A.2. Constants of the heat capacity equation, C_P (J/(mol K)) (Smith *et al.*, 2005)

Species	A	B x10^3	C x10^6	D x10^{-5}
CO	3.376	0.557	-	-0.031
H_2	3.249	0.422	-	0.083
CO_2	5.457	1.045	-	-1.157
H_2O	3.470	1.450	-	0.121
CH_4	1.702	9.081	-2.164	-
C_2H_6	1.131	19.225	-5.561	-
C_3H_8	1.213	28.785	-8.824	-
C_4H_{10}	1.935	36.915	-11.402	-
C_5H_{12}	2.464	45.351	-14.111	-
C_6H_{14}	3.025	53.722	-16.791	-
C_7H_{16}	3.57	62.127	-19.486	-
C_2H_4	1.424	14.394	-4.392	-
C_3H_6	1.637	22.706	-6.915	-
C_4H_8	1.967	31.63	-9.873	-
C_5H_{10}	2.691	39.753	-12.447	-
C_6H_{12}	3.22	48.189	-15.157	-
C_7H_{14}	3.768	56.588	-17.847	-

Table A.3. Reference viscosities and temperatures of species, and Sutherland constants (Crane, 1982)

Species	μ_0 (cP)	T_0 (K)	S
CO	1.72×10^{-2}	288.15	1.18×10^{2}
H_2	8.70×10^{-3}	273.15	7.20×10^{1}
H_2O	1.12×10^{-2}	350.00	1.06×10^{3}
CH_4	1.20×10^{-3}	273.15	1.98×10^{2}
Air	1.83×10^{-2}	291.15	1.20×10^{2}

Table A.4. Sum of structural volume increments of components (Poling *et al.*, 2004)

Species	$\sum \vartheta$
CO	18
H_2	6.12

Table A.5. Molecular mass of species (Smith *et al.*, 2005)

Species	Molecular Mass
CO	28.01
H_2	2.016
CO_2	44.01
H_2O	18.015
Air	28.851
CH_4	16.043
C_2H_6	30.07
C_3H_8	44.097
C_4H_{10}	58.123
C_5H_{12}	72.15
C_6H_{14}	86.177
C_7H_{16}	100.204
C_2H_4	28.054
C_3H_6	42.081
C_4H_8	56.108
C_5H_{10}	70.134
C_6H_{12}	84.161
C_7H_{14}	98.188

REFERENCES

Aasberg-Petersen, K., T.S. Christensen, I. Dybkjaer , J. Sehested, M. Ostberg, R. M. Coertzen, M. J. Keyser and A.P. Steynberg, 2004, "Synthesis gas production for FT synthesis", in A. Steynberg and M. Dry (eds.), *Fischer Tropsch Technology, Studies in Surface Science and Catalysis 152*, pp. 258-405, Elsevier

Avcı, A.K., D.L. Trimm and M. Karakaya, 2009, "Microreactor catalytic combustion for chemicals processing", *Catalysis Today*, doi:10.1016/j.cattod.2009.01.046

Bird, R.B., W.E. Stewart and E.N. Lightfoot, 2007, *Transport Phenomena*, 2^{nd} edn., Wiley, New York

Callagan, C.A., 2006, *Kinetics and Catalysis of the Water-Gas-Shift Reaction: A Microkinetic and Graph Theoretic Approach*, Ph.D. Thesis, Worcester Polytechnic Institute

Crane Co., 1982, *Flow of Fluids, Through valves, fittings and pipe, Technical Paper No. 410M* , New York, USA

Crude Oil and Commodity Prices, 2010, http://www.oil-price.net/

Dancuart, L. P., R. de Haan and A. de Klerk, 2004, "Processing of Primary Fischer-Tropsch Products", in A. Steynberg and M. Dry (eds.), *Fischer Tropsch Technology, Studies in Surface Science and Catalysis 152*, pp. 482-532, Elsevier

Donnelly T. J. and C. Satterfield, 1989, "Product Distributions of The Fischer-Tropsch Synthesis on Precipitated Iron Catalysts", *Applied Catalysis*, Vol. 52, pp. 93

Dry, M.E., 1999, "Fischer-Tropsch reactions and the environment", *Applied Catalysis*, Vol. 189, pp. 185-190

Dry, M.E., 2002, "The Fischer-Tropsch process: 1950-2000", *Catalysis Today*, Vol. 71,

pp. 227-241

Dry, M.E., 2004, "Chemical concepts used for engineering purposes", in A. Steynberg and M. Dry (eds.), *Fischer Tropsch Technology, Studies in Surface Science and Catalysis 152*, pp. 196-257, Elsevier

Dry. M. E. and A. Steynberg, 2004, "Commercial FT Process Applications", in A. Steynberg and M. Dry (eds.), *Fischer Tropsch Technology, Studies in Surface Science and Catalysis 152*, pp. 406-481, Elsevier

Ehrfeld, W., V. Hessel and V. Haverkamp, 1999, "Microreactors", in *Ullman's Encyclopedia of Industrial Chemistry*, Wiley-VCH, Weinheim

Enright R., C. Eason, T. Dalton, M. Hodes, T. Salamon, P. Kolodner and T. Krupenkin, 2006, "Friction factors and nusselt numbers in microchannels with superhydrophobic walls", *Proceedings of ICNMM2006, Fourth International Conference on Nanochannels, Microchannels and Minichannels*, June 19-21, 2006, Limerick, Ireland

Fan, Y., X. Zhong, J. Liu, T. Wang, Y. Zhang and Z. Cheng, 2007, "A Study of Effects of Coolants on Heat Transfer Capability of On-chip Cooling with CNT Microfin Architectures by Using CFD Simulation", *HDP'07: Proceedings of the 2007 International Symposium on High Density Packaging and Microsystem Integration*, June 26-28, 2007, Shanghai, China,

Fichtner, M., J. Mayer, D. Wolf and K. Schubert, 2001, "Microstructured Rhodium Catalysts for the Partial Oxidation of Methane to Syngas under Pressure", *Industrial & Engineering Chemistry Research*, Vol. 40, pp. 3475-3483

Fogler, H.S., 2006, *Elements of Chemical Reaction Engineering*, 4^{th} edn., Pearson, USA

Fox, J. M., 1993, "The Different Catalytic Routes for Methane Valorization: An Assessment Of Processes For Liquid Fuels", *Catalysis Reviews: Science and Engineering*,

Vol. 35, pp. 169-212

Geankoplis, C.J., 2003, *Transport Processes and Separation Process Principles*, 4^{th} edn., Prentice Hall, New Jersey

Geyer, K., J.D.C. Codee and P.H. Seeberger, 2006, "Microreactors as Tools for Synthetic ChemistsThe Chemists Round-Bottomed Flask of the 21^{st} Century?", *Chemistry European Journal*, Vol. 12, pp. 8434 8442

Gregor, J.H., 1990, "Fischer-Tropsch Products as Liquid Fuels or Chemicals. An Economical Evaluation", *Catalysis Letters*, Vol. 7, pp. 317-332

Harris C., M. Despa and K. Kelly, 2000, "Design and Fabrication of a Cross Flow Micro Heat Exchanger", *Journal Of Microelectromechanical Systems*, Vol. 9, No. 4, pp. 502-508

Hasebe, S., 2004, "Design and Operation of Micro-Chemical Plants - Bridging The Gap Between Nano, Micro and Macro Technologies", *Computers & Chemical Engineering*, Vol. 29, pp. 57-64

Holladay, J.D., Y. Wang and E. Jones, 2004, "Review of Developments in Portable Hydrogen Production Using Microreactor Technology", *Chemical Reviews*, Vol. 104, No. 10, pp. 4767-4789

Iglesia, E., S.C. Reyes and R.J. Madon, 1991, "Transport-Enhanced α-olefin Re-Adsorption Pathways Ru-Catalyzed Hydrocarbon Synthesis", *The Journal of Catalysis*, Vol. 129, pp. 238-256

Incropera, F.P., D.P. Dewitt, T.L. Bergman and A.S. Lavine, 2007, *Introduction to Heat Transfer*, 5^{th} edn., Wiley, New York

Jensen, K.F., 2001, "Microreaction engineering - is small better?", *Chemical Engineering Science*, Vol. 56, pp. 293-303

Ji, Y.-Y., H.-W. Xiang, J.-L. Yang, Y.-Y. Xu, Y.-W. Li and B. Zhong, 2001, "Effect of reaction conditions on the product distribution during Fischer-Tropsch synthesis over an industrial Fe-Mn catalyst", *Applied Catalysis A: General*, Vol. 214, pp. 77-86

Keyser, M.J., R. C. Everson and R. L. Espinoza, 2000, "Fischer-Tropsch Kinetic Studies with Cobalt-Manganese Oxide Catalysts", *Ind. Eng. Chem. Res.*, Vol. 39, pp. 48-54

Kiwi-Minsker, L. and Renken, A., 2005, "Microstructured reactors for catalytic reactions", *Catalysis Today*, Vol.110, pp. 2-14

Kolb, G. and V. Hessel, 2004, "Microstructured reactors for gas phase reactions", *Chemical Engineering Journal*, Vol. 98, pp. 1-38

Krieger, F.J., 1951, *Calculation of the viscosity of gas mixtures*, The Rand Corporation, California

Kuipers, E. W., C. Scheper, J. H. Wilson, and H. Oosterbeek, 1996, "Non-ASF Product Distributions Due to Secondary Reactions during Fischer-Tropsch Synthesis", *The Journal of Catalysis*, Vol.158, pp. 288

Lee, P.S., S. V. Garimella and D. Liu, 2005, "Investigation of heat transfer in rectangular microchannels", *International Journal of Heat and Mass Transfer*, Vol. 48, pp. 1688-1704

Lox, E.S. and G.F. Froment, 1993, "Kinetics of the Fischer-Tropsch Reaction on a Precipitated Promoted Iron Catalyst. 1. Experimental Procedure and Results", *Industrial & Engineering Chemistry Research*, Vol. 32, No. 1, pp. 61-70

Lu, Y. and T. Lee, 2007, "Influence of the Feed Gas Composition on the Fischer-Tropsch Synthesis in Commercial Operations", *Journal of Natural Gas Chemistry*, Vol. 16, pp. 329-341

Mazonne, L.C.A. and F.A.N. Fernandes, 2006, "Modeling of Fischer-Tropsch Synthesis in a Tubular Reactor", *Latin American Applied Research*, Vol. 36, pp. 141-148

Norton, D.G. and D. G. Vlachos, 2003, "Combustion characteristics and flame stability at the microscale: a CFD study of premixed methane/air mixtures", *Chemical Engineering Science*, Vol. 58, pp. 4871-4882

Norton, D.G. and D. G. Vlachos, 2004, "A CFD study of propane/air microflame stability", *Combustion and Flame*, Vol. 138, pp. 97-107

Peterson, R.B., 1999, "Numerical Modeling of Conduction Effects in Microscale Counterflow Heat Exchangers", *Microscale Thermophysical Engineering*, Vol. 3, pp. 17-30

Poling, B.E., J.M. Prausnitz and J.P. O'Connell, 2004, *The Properties of Gases and Liquids*, 5^{th} edn., McGraw Hill, USA

Schulz, H., 1999, "Short history and present trends of Fischer-Tropsch synthesis", *Applied Catalysis A: General*, Vol. 186, pp. 3-12

Schulz, H. and M. Claeys, 1999, "Kinetic modelling of Fischer-Tropsch product distributions", *Applied Catalysis A: General*, Vol. 186, pp. 91-107

Seris, E.L.C., G. Abramowitz, A.M. Johnston, and B.S.Haynes, 2008, "Scaleable, microstructured plant for steam reforming of methane", *Chemical Engineering Journal*, Vol.135, pp.9-16

Sinnot, R. K., 2003, *Coulson's & Richardson's Chemical Engineering, Design*, Vol. 6., 3^{rd} edn., Butterworth-Heinemann, London

Shen, W.J., J.L. Zhou and B.J. Zhang, 1996, "Intraparticle diffusion effects in Fischer-Tropsch Synthesis, I. Modeling of Diffusion and Reaction", *Journal of Natural Gas Chemistry*, Vol. 5, No. 1, pp. 59- 68

Smith, J.M., H.C. Van Ness and M.M. Abbott, 2005, *Introduction to Chemical Engineering Thermodynamics*, 7^{th} edn., McGraw Hill, Singapore

Steinke, M.E. and S. G. Kandlikar, 2004, "Single-Phase Heat Transfer Enhancement Techniques in Microchannel and Minichannel Flows", *Microchannels and Minichannels - 2004*, June 17-19, Rochester, New York, USA

Steynberg, A. P., 2004, "Introduction to Fischer-Tropsch Technology", in A. Steynberg and M. Dry (eds.), *Fischer Tropsch Technology, Studies in Surface Science and Catalysis 152*, pp. 1-63, Elsevier

Steynberg, A., M. Dry, B. H. Davis and B. B. Breman, 2004, "Fischer-Tropsch Reactors", in A. Steynberg and M. Dry (eds.), *Fischer Tropsch Technology, Studies in Surface Science and Catalysis 152*, pp. 64-195, Elsevier

Stutz, M.J. and D. Poulikakos, 2005, "Effects of microreactor wall heat conduction on the reforming process of methane", *Chemical Engineering Science*, Vol. 60, pp. 6983-6997

Tonkovich, A. L. Y., B. Yang, S. T. Perry, S. P. Fitzgerald and Y. Wang, 2007, "From seconds to milliseconds to microseconds through tailored microchannel reactor design of a steam methane reformer", *Catalysis Today*, Vol. 120, pp. 21-29

Tonkovich, A., D. Kuhlmann, A. Rogers, J. Mcdaniel, S. Fitzgerald, R. Arora and T. Yuschak, 2005, "Microchannel Technology Scale-Up To Commercial Capacity", *Trans IChemE, Part A, Chemical Engineering Research and Design*, Vol.83(A6), pp. 634-639

Tonkovich, A. Y., S. Perry, Y. Wang, D. Qiua, T. La Plantea and W.A. Rogers,2004, "Microchannel process technology for compact methane steam reforming", *Chemical Engineering Science*, Vol. 59, pp. 4819 - 4824

Tonkovich, A. Y., J.L. Zilka, M.J. LaMont, Y. Wang and R.S. Wegeng, 1999, "Mi-

crochannel reactors for fuel processing applications. I. Water gas shift reactor", *Chemical Engineering Science*, Vol. 54, pp. 2947-2951

Van der Laan, G.P, 1999, *Kinetics, Selectivity and Scale Up of the Fischer-Tropsch Synthesis*, Ph.D. Thesis, University of Groningen

Van der Laan, G.P. and A. A. C. M. Beenackers, 1999a, "Hydrocarbon Selectivity Model for the Gas-Solid Fischer-Tropsch Synthesis on Precipitated Iron Catalysts", *Industrial & Engineering Chemistry Research*, Vol. 38, pp. 1277-1290

Van der Laan, G.P. and A.A.C.M. Beenackers, 1999b, "Kinetics and Selectivity of the Fischer Tropsch Synthesis: A Literature Review", *Catalysis Reviews*, Vol. 41, Issue 3, pp. 255-318

Van Male, P., M.H.J.M. de Croon, R.M. Tiggelaar, A. van den Berg and J.C. Schouten, 2004, "Heat and Mass Transfer In A Square Microchannel with Asymmetric Heating", *International Journal of Heat and Mass Transfer*, Vol. 47, pp. 87-99

Veser, G. and J. Frauhammer, 2000, "Modelling Steady State and Ignition During Catalytic Methane Oxidation in a Monolith Reactor", *Chemical Engineering Science*, Vol. 55, pp. 2271-2286.

Veser, G., 2001, "Experimental and Theoretical Investigation of H2 Oxidation in a High-Temperature Catalytic Microreactor", *Chemical Engineering Science*, Vol. 56, pp. 1265-1273

Visconti, C.G., E. Tronconi, L. Lietti, R. Zennaro and P. Forzatti, 2007, "Development of a complete kinetic model for the FischerTropsch synthesis over Co/Al_2O_3 catalysts", *Chemical Engineering Science*, Vol. 62, pp. 5338-5343

Wang Y.N., W. P. Ma, Y.J. Lu, J. Yang, Y.Y. Xu, H.W. Xiang, Y.W. Li, Y.L. Zhao and B.J. Zhang, 2003, "Kinetics modelling of Fischer-Tropsch synthesis over an industrial Fe-Cu-K catalyst", *Fuel*, Vol. 82, pp. 195-213

Yang, J., Y. Liu, J. Chang, Y.N. Wang, L. Bai, Y.Y. Xu, H.W. Xiang, Y.W. Li, and B. Zhong, 2003, "Detailed Kinetics of Fischer-Tropsch Synthesis on an Industrial Fe-Mn Catalyst", *Industrial & Engineering Chemistry Research*, Vol. 42, pp. 5066-5090

Zanfir, M. and A. Gavriilidis, 2001, "Modelling of a catalytic plate reactor for dehydrogenation-combustion coupling", *Chemical Engineering Science*, Vol. 56, pp. 2671-2683